Ziv–Zakai Bounds on Time Delay Estimation in Unknown Convolutive Random Channels

Brian M. Sadler, *Fellow, IEEE*, Ning Liu, *Student Member, IEEE*, and Zhengyuan Xu, *Senior Member, IEEE*

***Abstract*—Using the Ziv–Zakai bound (ZZB) methodology, we develop a Bayesian mean-square error bound on time delay estimation (TDE) in convolutive random channels, and compare it with time delay estimator performance and a Cramér–Rao bound. The channel is modeled as a tapped delay line, whose taps are Gaussian random variables that may be nonzero mean and correlated, a model widely adopted in many applications such as wideband fading in a multipath channel. The time delay has a uniform prior distribution. A ZZB is developed that incorporates the prior on the random time delay, as well as the convolutive random Gaussian channel, and does not assume the receiver has knowledge of the channel realization. The ZZB provides good performance prediction for maximum *a posteriori* (MAP) time delay estimation, tracking the low, medium, and high signal-to-noise ratio (SNR) regimes. The convolutive channel model includes important special cases, such as narrowband Gaussian channels corresponding to Rayleigh/Rician fading, wideband multipath channels with a power decay profile (such as exponential decay), and known channels. We show that the associated Cramér–Rao bound is tight only at high SNR, whereas the ZZB predicts threshold behavior and TDE breakdown as the SNR decreases. When compared to a ZZB that assumes knowledge of the channel realization, the ZZB developed here provides a more realistic and tighter bound, revealing the performance loss due to lack of channel knowledge. The MAP estimator incorporates knowledge of the channel statistics, and so performs much better than a maximum likelihood estimator that minimizes mean square error but does not use knowledge of the random channel statistics. Several examples illustrate the estimator and bound behaviors.**

***Index Terms*—Bayesian estimation, convolutive fading channel, Cramér–Rao bound, error analysis, MAP estimation, MLE, time delay estimation, Ziv–Zakai bound.**

I. Introduction

TIME DELAY estimation (TDE) is fundamental in many applications, including ranging, synchronization, communications, geolocation, and array processing. The Cramér–Rao bound (CRB) has been extensively applied for bounding TDE performance in the case of a deterministic channel model, e.g., Yau and Bresler developed CRBs for superimposed and delayed parameterized signals [2], and that approach is readily adapted to the case of TDE in a known deterministic multipath channel [3]. However, the encountered channel is often wideband, random, and unknown. And, the CRB is only tight at high signal-to-noise ratios (SNRs). In this paper, we develop a Bayesian bound on TDE in convolutive random Gaussian channels that is suitable for a large range of SNRs, and we compare the bound with time delay estimator performance. The Gaussian random channel model is widely adopted, for example, for narrow band and wideband wireless communication fading channels [4]–[6].

The first part of the paper is devoted to derivation of a Bayesian mean square error (MSE) bound on TDE using the Ziv–Zakai bound (ZZB) approach [7], [8]. The ZZB is among the best MSE bounds for predicting optimal estimation performance over a wide range of SNRs; e.g., see Van Trees and Bell and references therein [9]. A survey of TDE bounds is given in [10]. ZZBs on TDE have been developed for narrowband frequency hopping channels [11], parallel narrowband channels [12], [13], and for ultra-wideband signals in additive white Gaussian noise (AWGN) channels [14]. Bayesian bounds have also been developed by Weinstein and Weiss and applied to TDE [9], [10], [15].

We assume that the receiver knows the channel distribution, but does not know the channel realization. The signal is assumed known to the receiver, and the time delay has a uniform prior distribution. We have previously considered the case when the channel realization is assumed perfectly known at the receiver to develop a ZZB on TDE [16], sometimes called the perfect measurement based lower bound [17]. The ZZB developed here represents a more realistic and tighter bound, and comparison of our new results with [16] reveals the TDE accuracy penalty associated with the unknown channel. Our ZZB derivation differs considerably from that in [16]. Here, both the multipath channel taps and noise are treated as Gaussian random variables. The log-likelihood ratio (LLR) for the associated hypothesis test in the ZZB derivation is shown to follow a general quadratic form of a Gaussian random vector. We then find the probability density function (pdf) of the LLR via a moment generating function (MGF) approach, that in turn leads to the minimum detection error probability expression needed to complete the ZZB derivation.

We compare the ZZB with a CRB, as well as the performance of a maximum *a posteriori* (MAP) time delay estimator. With a uniform prior on the time delay parameter, the Bayesian CRB is inapplicable due to the violation of regularity conditions, so we turn to the expected value of a conditional CRB [9], conditioned on the random Gaussian channel. We show that the ZZB provides much better prediction of the MAP estimator performance for high, medium, and low SNR regimes, than does the CRB. We also compare to a minimum mean-square error (MMSE) time delay estimator. The MAP estimator exploits knowledge of the

Manuscript received August 05, 2009; accepted December 18, 2009. Date of publication January 26, 2010; date of current version April 14, 2010. The associate editor coordinating the review of this manuscript and approving it for publication was Dr. Ali Ghrayeb. This work was supported in part by the Army Research Laboratory CTA on Communications and Networks under Grant DAAD19-01-2-0011. Some preliminary results were presented at the IEEE Sensor Array and Multichannel Signal Processing Workshop, Darmstadt, Germany, July 2008 [1].

B. M. Sadler is with the Army Research Laboratory, RDRL-CIN-T, Adelphi, MD 20783 USA (e-mail: bsadler@arl.army.mil).

N. Liu and Z. Xu are with the Department of Electrical Engineering, University of California, Riverside, CA 92521 USA (e-mail: dxu@ee.ucr.edu).

Digital Object Identifier 10.1109/TSP.2010.2041379

channel distribution, and so performs considerably better than the MMSE estimator that does not.

This paper is organized as follows. In Section II, the signal, channel, and receiver models are introduced. The received signal distribution is established in Section III, along with the setup for the ZZB derivation. The ZZB derivation and various cases occupy Sections IV through VII. In Section IV, development of the ZZB is facilitated via a MGF approach using quadratic forms of Gaussian random variables. The ZZB is analyzed asymptotically for both low and high SNRs in Section V, and a means to find the SNR thresholds is described. Some important special cases of the ZZB are then considered in Section VI, including the cases of memoryless random channels (flat fading) and known channels. A detailed road map for computation of the ZZB, as well as low and high SNR limiting cases, is provided in Section VII. In Section VIII, we compare the ZZB against Bayesian time delay estimation performance, and the CRB that is averaged over the random unknown channel. Numerical examples of estimation and the bounds are given in Section IX, followed by conclusions in Section X.

II. Signal and Channel Models

The transmitted signal is given by $p(t) = \sqrt{E_{\rm tx}}s(t)$, where $s(t)$ is normalized to have unit energy, so that $E_{\rm tx}$ is the transmitted signal energy. The signal propagates through a convolutive random channel, or tapped delay line, with fixed spacing T_t, given by

$$g(t) = \sqrt{G_0}\sum_{l=0}^{L-1}\alpha_l\delta(t-lT_t). \tag{1}$$

Here, G_0 is the total gain factor, L is the total number of taps, α_l is the gain for the $(l+1)$th tap, and let $\boldsymbol{\alpha} = [\alpha_1,\ldots,\alpha_L]^T$. We model $\boldsymbol{\alpha}$ as a Gaussian random vector with distribution denoted $\mathcal{N}(\boldsymbol{\mu}_\alpha, \boldsymbol{V})$, where $\boldsymbol{\mu}_\alpha$ is the mean vector and $\boldsymbol{V}$ is the covariance matrix. The channel is assumed to have unit power such that $\mathrm{tr}(\boldsymbol{\mu}_\alpha\boldsymbol{\mu}_\alpha^T+\boldsymbol{V}) = 1$, where tr is the trace operator. Define $E_{\rm rx} \triangleq G_0E_{\rm tx}$ and denote the positive real propagation delay as t_0. The received signal is given by

$$\begin{aligned} y(t) &= \sqrt{E_{\rm rx}}\sum_{l=0}^{L-1}\alpha_l s(t-lT_t-t_0)+n(t)\\ &= \sqrt{E_{\rm rx}}\boldsymbol{\alpha}^T\boldsymbol{s}(t-t_0)+n(t) \end{aligned} \tag{2}$$

where

$$\begin{aligned} \boldsymbol{s}(t-t_0) = [&s(t-t_0), s(t-T_t-t_0),\ldots,\\ &s(t-(L-1)T_t-t_0)]^T, \end{aligned} \tag{3}$$

and $n(t)$ is AWGN with double sided spectral density $\sigma_n^2 = N_0/2$, from which the signal to noise ratio is defined as $\xi_b = E_{\rm rx}/\sigma_n^2$. We assume a uniform prior distribution for t_0 in $[0,T]$. The TDE problem is to estimate t_0, and we derive a ZZB for this beginning in the next section.

III. Development of the Ziv–Zakai Bound

The development of the ZZB links estimation of time delay t_0 to a hypothesis testing problem that discriminates a signal at two possible delays [7]. Let $\hat{t}_0$ be a time delay estimate. For a received signal $h(t)$ at one of the two possible delays $h(t-a)$ or $h(t-a-\Delta)$, where $\Delta > 0$ and $a, a+\Delta \in [0,T]$, the hypothesis test is given by

$$\begin{aligned} &\text{Decide } H_0\text{:}\quad t_0 = a \qquad \text{if } |\hat{t}_0-a| < |\hat{t}_0-a-\Delta|,\\ &\text{Decide } H_1\text{:}\quad t_0 = a+\Delta \quad \text{if } |\hat{t}_0-a| > |\hat{t}_0-a-\Delta|. \end{aligned} \tag{4}$$

Denote the estimation error by $\epsilon = \hat{t}_0 - t_0$, and let $P_e(a,a+\Delta)$ be the minimal probability of error achieved by the optimum detection scheme in making the above decision. If the two hypothesized delays are equally likely to occur, then the estimation MSE is lower bounded by [7]

$$\overline{\epsilon^2} \geq \frac{1}{T}\int_0^T \Delta\int_0^{T-\Delta} P_e(a,a+\Delta)da\,d\Delta. \tag{5}$$

In general, with equally likely hypotheses, $P_e(a,a+\Delta)$ is only a function of the offset Δ and not a. Thus, we will write $P_e(\Delta) = P_e(a,a+\Delta)$, and it follows that

$$\overline{\epsilon^2} \geq \frac{1}{T}\int_0^T \Delta(T-\Delta)P_e(\Delta)d\Delta. \tag{6}$$

Evaluation of the bound (6) relies on finding the minimal probability of error $P_e(\Delta)$ in making the hypothesis test. We will find $P_e(\Delta)$ by evaluating the LLR test, as follows. We find the conditional distribution of the received signal, conditioned on the channel realization. This is then averaged over the channel distribution, yielding the distribution of the received signal, reflecting the lack of knowledge of the channel at the receiver. The LLR is shown to depend quadratically on the received signal, and in Section IV we use a moment generating function approach to find an expression for the LLR distribution. Finally, $P_e(\Delta)$ is found using the LLR distribution.[1]

A. Received Signal Distribution

From (2), the received signal can be written as

$$y(t) = \sqrt{E_{\rm rx}}\boldsymbol{\alpha}^T\boldsymbol{s}_m + n(t) \tag{7}$$

where m takes the value 0 or 1 corresponding to hypotheses H_0 or H_1, respectively, and

$$\begin{aligned} \boldsymbol{s}_m &= \boldsymbol{s}(t-m\Delta)\\ &= [s(t-m\Delta), s(t-T_t-m\Delta),\ldots,\\ &\quad s(t-(L-1)T_t)-m\Delta]^T. \end{aligned}$$

Note that, in the context of developing the bound, the delay parameter t_0 in (3) has been replaced by $m\Delta$. We assume the duration of the observation window at the receiver T_0, is much larger

[1]Note that with a known channel, $P_e(\Delta)$ is equivalent to the error probability of an optimal detector for binary pulse position modulation (PPM), as a function of the relative delay Δ [16]. In our case, this involves averaging over the unknown random channel.

than the sum of T and the duration of the channel output waveform, where the output waveform duration is $(L-1)T_t$ plus the duration of transmitted signal $p(t)$. From (7), the distribution of $y(t)$ conditioned on channel gain $\boldsymbol{\alpha}$ and time delay $m\Delta$ is [4]

$$\begin{aligned} &p(y(t)|\boldsymbol{\alpha}, m\Delta) \\ &\quad = \mathcal{K}\exp\left[-\frac{1}{2\sigma_n^2}\int_{T_0}(y(t)-\sqrt{E_{\rm rx}}\boldsymbol{\alpha}^T\boldsymbol{s}_m)^2dt\right] \\ &\quad = \mathcal{K}\exp\left[-\frac{1}{2\sigma_n^2}\left(E_{\rm rx}\boldsymbol{\alpha}^T\boldsymbol{S}_{00}\boldsymbol{\alpha}-2\sqrt{E_{\rm rx}}\boldsymbol{r}_m^T\boldsymbol{\alpha}+I_y\right)\right] \quad (8)\end{aligned}$$

where $\mathcal{K}$ absorbs all of the integration constants independent of $\boldsymbol{\alpha}$ and $m\Delta$, and

$$\begin{aligned} \boldsymbol{S}_{m_1m_2} &\triangleq \int_{T_0}\boldsymbol{s}_{m_1}\boldsymbol{s}_{m_2}^Tdt, \quad \boldsymbol{r}_m \triangleq \int_{T_0}\boldsymbol{s}_m y(t)dt, \\ I_y &\triangleq \int_{T_0} y^2(t)dt, \end{aligned} \quad (9)$$

with $m, m_1, m_2 = \{0,1\}$. $\boldsymbol{S}_{mm} = \boldsymbol{S}_{00} = \boldsymbol{S}_{11}$ is a symmetric Toeplitz matrix independent of m. We also introduce the non-symmetric Toeplitz matrices $\boldsymbol{S}_{01}$ and $\boldsymbol{S}_{10}$, to be used in the ZZB development in Section III. If we denote the transmitted waveform autocorrelation by

$$\beta_\tau = \int_{T_o} s(t)s(t-\tau)dt$$

and define the $L \times L$ down-shifting matrix $\boldsymbol{J}$ whose first subdiagonal elements below the main diagonal are ones while all others are zeros, then these matrices can be compactly written as [16]

$$\begin{aligned} \boldsymbol{S}_{00} = \boldsymbol{S}_{11} &= \sum_{k=-(L-1)}^{L-1}\beta_{-kT_t}\boldsymbol{J}^k \\ \boldsymbol{S}_{01} = \boldsymbol{S}_{10}^T &= \sum_{k=-(L-1)}^{L-1}\beta_{\Delta-kT_t}\boldsymbol{J}^k \end{aligned} \quad (10)$$

where $\boldsymbol{J}^{-1} \triangleq \boldsymbol{J}^T$, $\boldsymbol{J}^0 \triangleq \boldsymbol{I}$.

Next, we average (8) over the channel $\boldsymbol{\alpha}$, given by

$$\begin{aligned} &p(y(t)\,|\,m\Delta) \\ &\quad = E_\alpha\{p(y(t)\,|\,\boldsymbol{\alpha}, m\Delta)\} \\ &\quad = \mathcal{K}E_\alpha\left\{\exp\left[-\frac{1}{2\sigma_n^2}\left(E_{\rm rx}\boldsymbol{\alpha}^T\boldsymbol{S}_{00}\boldsymbol{\alpha}-2\sqrt{E_{\rm rx}}\boldsymbol{r}_m^T\boldsymbol{\alpha}+I_y\right)\right]\right\}. \end{aligned} \quad (11)$$

The expected value of the exponential of a quadratic form of the normal random vector $\boldsymbol{\alpha}$ can be obtained from its moment generating function [18]. Let Q be the exponent in (11), given by

$$Q = -\frac{1}{2\sigma_n^2}\left(E_{\rm rx}\boldsymbol{\alpha}^T\boldsymbol{S}_{00}\boldsymbol{\alpha}-2\sqrt{E_{\rm rx}}\boldsymbol{r}_m^T\boldsymbol{\alpha}+I_y\right).$$

Using (100) in Appendix I, with $s=1$, then we find

$$p(y(t)\,|\,m\Delta) = \mathcal{K}|\boldsymbol{X}|^{-\frac{1}{2}}\exp\left\{\frac{1}{2}\boldsymbol{v}_m^T\boldsymbol{X}^{-1}\boldsymbol{v}_m + c_m\right\} \quad (12)$$

where

$$\boldsymbol{X} = \boldsymbol{I} + \frac{E_{\rm rx}}{\sigma_n^2}\boldsymbol{V}^{\frac{1}{2}}\boldsymbol{S}_{00}\boldsymbol{V}^{\frac{1}{2}} = \boldsymbol{I} + \xi_b\boldsymbol{V}^{\frac{1}{2}}\boldsymbol{S}_{00}\boldsymbol{V}^{\frac{1}{2}} \quad (13)$$

and ξ_b is the SNR as defined in Section II. The received signal is embedded in $\boldsymbol{v}_m$ and c_m, given by

$$\begin{aligned} \boldsymbol{v}_m &= \frac{\sqrt{E_{\rm rx}}}{\sigma_n^2}\boldsymbol{V}^{\frac{1}{2}}\boldsymbol{r}_m - \frac{E_{\rm rx}}{\sigma_n^2}\boldsymbol{V}^{\frac{1}{2}}\boldsymbol{S}_{00}\boldsymbol{\mu}_\alpha \\ c_m &= \frac{\sqrt{E_{\rm rx}}}{\sigma_n^2}\boldsymbol{\mu}_\alpha^T\boldsymbol{r}_m - \frac{E_{\rm rx}}{2\sigma_n^2}\boldsymbol{\mu}_\alpha^T\boldsymbol{S}_{00}\boldsymbol{\mu}_\alpha - \frac{I_y}{2\sigma_n^2}. \end{aligned}$$

Using $\boldsymbol{v}_m$ and c_m, (12) can be expressed as a function of $\boldsymbol{r}_m$, given by

$$p(y(t)\,|\,m\Delta) = \mathcal{K}|\boldsymbol{X}|^{-\frac{1}{2}}\exp\left\{\boldsymbol{r}_m^T\boldsymbol{W}\boldsymbol{r}_m + \boldsymbol{h}^T\boldsymbol{r}_m + \tilde{c}\right\} \quad (14)$$

where

$$\begin{aligned} \tilde{c} &= \frac{E_{\rm rx}^2}{2\sigma_n^4}\boldsymbol{\mu}_\alpha^T\boldsymbol{S}_{00}\boldsymbol{V}^{\frac{1}{2}}\boldsymbol{X}^{-1}\boldsymbol{V}^{\frac{1}{2}}\boldsymbol{S}_{00}\boldsymbol{\mu}_\alpha - \frac{E_{\rm rx}}{2\sigma_n^2}\boldsymbol{\mu}_\alpha^T\boldsymbol{S}_{00}\boldsymbol{\mu}_\alpha - \frac{I_y}{2\sigma_n^2} \\ \boldsymbol{W} &= \frac{E_{\rm rx}}{2\sigma_n^4}\boldsymbol{V}^{\frac{1}{2}}\boldsymbol{X}^{-1}\boldsymbol{V}^{\frac{1}{2}} = \frac{\xi_b^2}{2E_{\rm rx}}\boldsymbol{V}^{\frac{1}{2}}\boldsymbol{X}^{-1}\boldsymbol{V}^{\frac{1}{2}} \quad (15) \\ \boldsymbol{h} &= \frac{\sqrt{E_{\rm rx}}}{\sigma_n^2}\boldsymbol{\mu}_\alpha - \frac{\sqrt{E_{\rm rx}}E_{\rm rx}}{\sigma_n^4}\boldsymbol{V}^{\frac{1}{2}}\boldsymbol{X}^{-1}\boldsymbol{V}^{\frac{1}{2}}\boldsymbol{S}_{00}\boldsymbol{\mu}_\alpha \\ &= \frac{\xi_b}{\sqrt{E_{\rm rx}}}\left(\boldsymbol{I}-\xi_b\boldsymbol{V}^{\frac{1}{2}}\boldsymbol{X}^{-1}\boldsymbol{V}^{\frac{1}{2}}\boldsymbol{S}_{00}\right)\boldsymbol{\mu}_\alpha = \boldsymbol{H}\boldsymbol{\mu}_\alpha. \quad (16)\end{aligned}$$

Note that $\tilde{c}$ does not depend on m, i.e., it does not depend on the hypothesis choice. Note also that $\boldsymbol{h} = \boldsymbol{0}$ in the zero-mean channel case, i.e., when $\boldsymbol{\mu}_\alpha = \boldsymbol{0}$.

B. Log-Likelihood Ratio Test

We can now use the received signal distribution in (14) to evaluate the likelihood ratio (LR) for the hypothesis test. The LR to decide on hypothesis H_m, $m = 0, 1$, is

$$\Lambda \triangleq \frac{p(y(t)\,|\,0)}{p(y(t)\,|\,\Delta)} \underset{H_1}{\overset{H_0}{\gtrless}} 1. \quad (17)$$

Because $\tilde{c}$ in (14) does not depend on the hypothesis choice, then it will not affect the error probability of the hypothesis test and can be dropped. Consequently, employing (14), the LLR becomes

$$\begin{aligned} \mathcal{L} \triangleq \ln\Lambda &= \ln p(y(t)\,|\,0) - \ln p(y(t)\,|\,\Delta) \\ &= \boldsymbol{r}_0^T\boldsymbol{W}\boldsymbol{r}_0 - \boldsymbol{r}_1^T\boldsymbol{W}\boldsymbol{r}_1 + \boldsymbol{h}^T\boldsymbol{r}_0 - \boldsymbol{h}^T\boldsymbol{r}_1 \\ &= \boldsymbol{r}^T\boldsymbol{\Psi}\boldsymbol{r} + \boldsymbol{g}^T\boldsymbol{r} \\ &\underset{H_1}{\overset{H_0}{\gtrless}} 0 \end{aligned} \quad (18)$$

where

$$\boldsymbol{r} = \begin{bmatrix}\boldsymbol{r}_0 \\ \boldsymbol{r}_1\end{bmatrix} \quad \boldsymbol{\Psi} = \begin{bmatrix}\boldsymbol{W} & \boldsymbol{0} \\ \boldsymbol{0} & -\boldsymbol{W}\end{bmatrix}$$
$$\boldsymbol{g} = \begin{bmatrix}\boldsymbol{h} \\ -\boldsymbol{h}\end{bmatrix} = \begin{bmatrix}\boldsymbol{H}\boldsymbol{\mu}_\alpha \\ -\boldsymbol{H}\boldsymbol{\mu}_\alpha\end{bmatrix} = \boldsymbol{G}\boldsymbol{\mu}_\alpha. \quad (19)$$

An error occurs if $\mathcal{L} < 0 \,|\, m = 0$, or if $\mathcal{L} > 0 \,|\, m = 1$. Thus, the hypothesis test minimum error probability can be written as

$$\begin{aligned} P_e(\Delta) &= \Pr\{\mathcal{L} < 0 \,|\, H_0\} Pr\{H_0\} \\ &\quad + \Pr\{\mathcal{L} > 0 \,|\, H_1\} \Pr\{H_1\} \\ &= \frac{1}{2} \Pr\{\mathcal{L} < 0 \,|\, H_0\} + \frac{1}{2} \Pr\{\mathcal{L} > 0 \,|\, H_1\} \end{aligned} \quad (20)$$

where the second equality assumes equally likely hypotheses. Let $\mathcal{L}_m \triangleq \mathcal{L} \,|\, H_m$, and $\tilde{\boldsymbol{r}}_m \triangleq \boldsymbol{r} \,|\, H_m$. Then (18) and (20) become

$$\mathcal{L}_m = \tilde{\boldsymbol{r}}_m^T \boldsymbol{\Psi} \tilde{\boldsymbol{r}}_m + \boldsymbol{g}^T \tilde{\boldsymbol{r}}_m \quad (21)$$

$$P_e(\Delta) = \frac{1}{2} \Pr\{\mathcal{L}_0 < 0\} + \frac{1}{2} \Pr\{\mathcal{L}_1 > 0\}. \quad (22)$$

Our goal now is to evaluate the probabilities in (22), in order to use $P_e(\Delta)$ in the ZZB expression (6). In the next subsection we find the distribution of $\tilde{\boldsymbol{r}}_m$. Then, in the next section, we derive the distribution of $\mathcal{L}_m$ from which the probabilities are obtained.

C. The Distribution of $\tilde{\boldsymbol{r}}_m$

Using (9) and (7) conditioned on H_0, then $\boldsymbol{r}_0$ and $\boldsymbol{r}_1$ can be expressed as

$$\begin{aligned} \boldsymbol{r}_0 \,|\, H_0 &= \int_{T_0} \boldsymbol{s}_0 \left[\sqrt{E_{\rm rx}} \boldsymbol{\alpha}^T \boldsymbol{s}_0 + n(t) \right] dt \\ &= \sqrt{E_{\rm rx}} \left(\int_{T_0} \boldsymbol{s}_0 \boldsymbol{s}_0^T dt \right) \boldsymbol{\alpha} + \int_{T_0} \boldsymbol{s}_0 n(t) dt \\ &= \sqrt{E_{\rm rx}} \boldsymbol{S}_{00} \boldsymbol{\alpha} + \boldsymbol{z}_0 \end{aligned} \quad (23)$$

$$\begin{aligned} \boldsymbol{r}_1 \,|\, H_0 &= \int_{T_0} \boldsymbol{s}_1 \left[\sqrt{E_{\rm rx}} \boldsymbol{\alpha}^T \boldsymbol{s}_0 + n(t) \right] dt \\ &= \sqrt{E_{\rm rx}} \left(\int_{T_0} \boldsymbol{s}_1 \boldsymbol{s}_0^T dt \right) \boldsymbol{\alpha} + \int_{T_0} \boldsymbol{s}_1 n(t) dt \\ &= \sqrt{E_{\rm rx}} \boldsymbol{S}_{10} \boldsymbol{\alpha} + \boldsymbol{z}_1 \end{aligned} \quad (24)$$

where

$$\boldsymbol{z}_0 \triangleq \int_{T_0} \boldsymbol{s}_0 n(t) dt, \quad \boldsymbol{z}_1 \triangleq \int_{T_0} \boldsymbol{s}_1 n(t) dt.$$

Stacking $\boldsymbol{r}_0 \,|\, H_0$ and $\boldsymbol{r}_1 \,|\, H_0$ as in (19), we obtain

$$\begin{aligned} \tilde{\boldsymbol{r}}_0 &= \boldsymbol{r} \,|\, H_0 = \sqrt{E_{\rm rx}} \boldsymbol{R}_0 \boldsymbol{\alpha} + \boldsymbol{z}, \\ \boldsymbol{R}_0 &= \begin{bmatrix} \boldsymbol{S}_{00} \\ \boldsymbol{S}_{10} \end{bmatrix}, \quad \boldsymbol{z} = \begin{bmatrix} \boldsymbol{z}_0 \\ \boldsymbol{z}_1 \end{bmatrix}. \end{aligned} \quad (25)$$

Similarly, conditioned on H_1, we find

$$\tilde{\boldsymbol{r}}_1 = \boldsymbol{r} \,|\, H_1 = \sqrt{E_{\rm rx}} \boldsymbol{R}_1 \boldsymbol{\alpha} + \boldsymbol{z}, \boldsymbol{R}_1 = \begin{bmatrix} \boldsymbol{S}_{01} \\ \boldsymbol{S}_{00} \end{bmatrix}. \quad (26)$$

Therefore, under either hypothesis the data vector $\tilde{\boldsymbol{r}}_0$ or $\tilde{\boldsymbol{r}}_1$ is a linear combination of Gaussian vectors $\boldsymbol{\alpha}$ and $\boldsymbol{z}$, so that $\tilde{\boldsymbol{r}}_m$ follows a normal distribution as $\tilde{\boldsymbol{r}}_m \sim \mathcal{N}(\boldsymbol{\mu}_m, \boldsymbol{\Sigma}_m)$. Using (25) and (26), the mean and variance of $\tilde{\boldsymbol{r}}_m$ can be compactly expressed as

$$\begin{aligned} \boldsymbol{\mu}_m &= \sqrt{E_{\rm rx}} \boldsymbol{m}_m, \quad \boldsymbol{m}_m = \boldsymbol{R}_m \boldsymbol{\mu}_\alpha \\ \boldsymbol{\Sigma}_m &= E_{\rm rx} \left(\boldsymbol{R}_m \boldsymbol{V} \boldsymbol{R}_m^T + \xi_b^{-1} \boldsymbol{\Gamma} \right) \end{aligned} \quad (27)$$

where

$$\boldsymbol{\Gamma} = E\{\boldsymbol{z}\boldsymbol{z}^T\}/\sigma_n^2 = \begin{bmatrix} \boldsymbol{S}_{00} & \boldsymbol{S}_{01} \\ \boldsymbol{S}_{10} & \boldsymbol{S}_{00} \end{bmatrix} = [\, \boldsymbol{R}_0 \quad \boldsymbol{R}_1 \,]. \quad (28)$$

Thus, the probability density function (pdf) of the $2L$-dimensional Gaussian vector $\tilde{\boldsymbol{r}}_m$ can be written as

$$f_m(\boldsymbol{x}) = \frac{1}{(\sqrt{2\pi})^{2L} \,|\, \boldsymbol{\Sigma}_m \,|} \exp\left\{ -\frac{1}{2} (\boldsymbol{x} - \boldsymbol{\mu}_m)^T \boldsymbol{\Sigma}_m^{-1} (\boldsymbol{x} - \boldsymbol{\mu}_m) \right\}$$

which will be useful in the next section.

Note that with the distribution of $\tilde{\boldsymbol{r}}_m$, we can easily express the probabilities in (22) as

$$\begin{aligned} \Pr\{\mathcal{L}_0 < 0\} &= \Pr\{\boldsymbol{x} \in \{\boldsymbol{x} : \boldsymbol{x}^T \boldsymbol{\Psi} \boldsymbol{x} + \boldsymbol{g}^T \boldsymbol{x} < 0\}\} \\ &= \underbrace{\int \cdots \int}_{\text{2Lfold}} {}_{\boldsymbol{x} \in \{\boldsymbol{x} : \boldsymbol{x}^T \boldsymbol{\Psi} \boldsymbol{x} + \boldsymbol{g}^T \boldsymbol{x} < 0\}} f_0(\boldsymbol{x}) d\boldsymbol{x} \end{aligned} \quad (29)$$

$$\begin{aligned} \Pr\{\mathcal{L}_1 > 0\} &= \Pr\{\boldsymbol{x} \in \{\boldsymbol{x} : \boldsymbol{x}^T \boldsymbol{\Psi} \boldsymbol{x} + \boldsymbol{g}^T \boldsymbol{x} > 0\}\} \\ &= \underbrace{\int \cdots \int}_{\text{2Lfold}} {}_{\boldsymbol{x} \in \{\boldsymbol{x} : \boldsymbol{x}^T \boldsymbol{\Psi} \boldsymbol{x} + \boldsymbol{g}^T \boldsymbol{x} > 0\}} f_1(\boldsymbol{x}) d\boldsymbol{x}. \end{aligned} \quad (30)$$

However, these require finding the bounding set for $\boldsymbol{x}$ and evaluating the $2L$-dimensional integrals. In the next section, we introduce an MGF approach that results in a 2-dimensional integration and is much more computationally attractive.

IV. Evaluation of the ZZB Using the Moment Generating Function

Using the results from Section III, we can now evaluate the ZZB as follows. If we know the distribution of the log-likelihood ratio $\mathcal{L}_m$ in (21), it is straightforward to evaluate the probabilities in (22) via 1-dimensional integration, and then use the resulting $P_e(\Delta)$ to find the ZZB in (6). Note that $\mathcal{L}_m$ is a quadratic function of the Gaussian vector $\tilde{\boldsymbol{r}}_m$, and so no closed form is available for the distribution of $\mathcal{L}_m$. Consequently, we adopt an MGF approach to find it. The MGF of $\mathcal{L}_m$ is given by

$$\begin{aligned} \Theta_m(s) &\triangleq E_{\tilde{r}_m}\{\exp(s\mathcal{L}_m)\} \\ &= E_{\tilde{r}_m}\left\{ \exp\left[s \left(\tilde{\boldsymbol{r}}_m^T \boldsymbol{\Psi} \tilde{\boldsymbol{r}}_m + \boldsymbol{g}^T \tilde{\boldsymbol{r}}_m \right) \right] \right\}. \end{aligned} \quad (31)$$

We consider two alternative forms for $\Theta_m(s)$, which we refer to as the direct form and the compact form. The compact form relies on eigendecomposition, but does not require explicit matrix inversion as does the direct form. So, in general the compact form is preferred for numerical evaluation. However, the direct form will prove convenient to carry out asymptotic analysis in Section V. Further numerical details are deferred until Section VI.

A. MGF Direct Form

Applying (101) from Appendix I, and using the mean and variance of $\tilde{r}_m$ from (27), we can evaluate (31) to obtain

$$\Theta_m(s) = |\tilde{\boldsymbol{A}}_m(s)|^{-\frac{1}{2}} \exp\left\{ sk_m + \frac{1}{2}s^2 \tilde{\boldsymbol{p}}_m^T \tilde{\boldsymbol{A}}_m^{-1}(s)\boldsymbol{\Sigma}_m \tilde{\boldsymbol{p}}_m \right\} \tag{32}$$

where

$$\tilde{\boldsymbol{A}}_m(s) = \boldsymbol{I} - 2s\boldsymbol{\Sigma}_m\boldsymbol{\Psi}, \quad k_m = \boldsymbol{\mu}_m^T\boldsymbol{\Psi}\boldsymbol{\mu}_m + \boldsymbol{g}^T\boldsymbol{\mu}_m$$
$$\tilde{\boldsymbol{p}}_m = \boldsymbol{g} + 2\boldsymbol{\Psi}\boldsymbol{\mu}_m. \tag{33}$$

Setting $s = j2\pi f$, the Fourier transform of $\Theta_m(j2\pi f)$ yields the pdf of $\mathcal{L}_m$, and the probabilities $\Pr\{\mathcal{L}_0 < 0\}$ and $\Pr\{\mathcal{L}_1 > 0\}$ are given by

$$\Pr\{\mathcal{L}_0 < 0\} = \int_{-\infty}^{0}\int_{-\infty}^{\infty} \Theta_0(j2\pi f) e^{-j2\pi f u} df du \tag{34}$$

$$\Pr\{\mathcal{L}_1 > 0\} = \int_{0}^{\infty}\int_{-\infty}^{\infty} \Theta_1(j2\pi f) e^{-j2\pi f u} df du. \tag{35}$$

Substituting $\Pr\{\mathcal{L}_0 < 0\}$ and $\Pr\{\mathcal{L}_1 > 0\}$ into (22), the minimum error probability $P_e(\Delta)$ follows.

The fast Fourier transform (FFT) algorithm can be employed to approximate the continuous Fourier transform in the innermost integration in (34) and (35). However, to do this, then for each $s = 2\pi f$ we must compute the matrix inverse and determinant of $\tilde{\boldsymbol{A}}_m(s)$, which has high computational complexity. In the next subsection we use the eigendecomposition approach to derive a compact form for the MGF, leading to lower complexity. We also note that (32) will prove useful to carry out asymptotic analysis of the ZZB in Section V.

B. MGF Compact Form

Next we consider an alternative evaluation of the MGF, that relies on eigendecomposition. We begin with the LLR in (21). Using the definitions of $\boldsymbol{\Psi}$ and $\boldsymbol{g}$ in (19), it can be easily shown that $\boldsymbol{g}^T\boldsymbol{\Psi}^{-1}\boldsymbol{g} = 0$. Therefore, the LLR becomes

$$\mathcal{L}_m = \tilde{\boldsymbol{x}}_m^T\boldsymbol{\Psi}\tilde{\boldsymbol{x}}_m, \tilde{\boldsymbol{x}}_m = \tilde{\boldsymbol{r}}_m + \frac{1}{2}\boldsymbol{\Psi}^{-1}\boldsymbol{g}. \tag{36}$$

Note that $\tilde{\boldsymbol{x}}_m$ is a Gaussian random vector with variance $\boldsymbol{\Sigma}_m$, and whose mean is

$$\boldsymbol{\mu}_{xm} = \boldsymbol{\mu}_m + \frac{1}{2}\boldsymbol{\Psi}^{-1}\boldsymbol{g} = \left(\sqrt{E_{\rm rx}}\boldsymbol{R}_m + \frac{1}{2}\boldsymbol{\Psi}^{-1}\boldsymbol{G}\right)\boldsymbol{\mu}_\alpha.$$

We introduce the zero mean Gaussian random vector $\boldsymbol{u}_m$, obtained from $\tilde{\boldsymbol{x}}_m$ by the transformation

$$\tilde{\boldsymbol{x}}_m = \boldsymbol{\Sigma}_m^{\frac{1}{2}}\boldsymbol{P}_m\boldsymbol{u}_m + \boldsymbol{\mu}_{xm} = \boldsymbol{\Sigma}_m^{\frac{1}{2}}\boldsymbol{P}_m(\boldsymbol{u}_m + \boldsymbol{b}_m),$$

so that the variance of $\boldsymbol{u}_m$ is the identity matrix $\boldsymbol{I}$, and the vector $\boldsymbol{b}_m$ is a linear transformation of channel mean $\boldsymbol{\mu}_\alpha$ given by

$$\begin{aligned}\boldsymbol{b}_m &= \boldsymbol{P}_m^T\boldsymbol{\Sigma}_m^{-\frac{1}{2}}\boldsymbol{\mu}_{xm} \\ &= \boldsymbol{P}_m^T\boldsymbol{\Sigma}_m^{-\frac{1}{2}}\left(\sqrt{E_{\rm rx}}\boldsymbol{R}_m + \frac{1}{2}\boldsymbol{\Psi}^{-1}\boldsymbol{G}\right)\boldsymbol{\mu}_\alpha.\end{aligned} \tag{37}$$

In this transformation, $\boldsymbol{P}_m$ is a unitary matrix in the eigendecomposition of the symmetric matrix given by

$$\boldsymbol{\Sigma}_m^{\frac{1}{2}}\boldsymbol{\Psi}\boldsymbol{\Sigma}_m^{\frac{1}{2}} = \boldsymbol{P}_m \mathrm{diag}\{\lambda_1, \ldots, \lambda_J, -\lambda_{J+1}, \ldots, -\lambda_{2L}\}\boldsymbol{P}_m^T. \tag{38}$$

From the structure of $\boldsymbol{\Psi}$ and the fact that $\boldsymbol{W}$ is positive definite, it follows that $\lambda_k \geq 0$ for all k.

From this, the elements u_{mk} of $\boldsymbol{u}_m$ are independent Gaussian random variables, each with zero mean and unit variance. It follows that (36) can be written as

$$\begin{aligned}\mathcal{L}_m &= (\boldsymbol{u}_m + \boldsymbol{b}_m)^T \\ &\quad \times \mathrm{diag}\{\lambda_1, \ldots, \lambda_J, -\lambda_{J+1}, \ldots, -\lambda_{2L}\}(\boldsymbol{u}_m + \boldsymbol{b}_m) \quad (39) \\ &= \sum_{k=1}^{J}\lambda_k(u_{mk} + b_{mk})^2 - \sum_{k=J+1}^{2L}\lambda_k(u_{mk} + b_{mk})^2 \quad (40)\end{aligned}$$

where b_{mk} is the kth element of $\boldsymbol{b}_m$.

The MGF is now obtained by using (39) in (102) from Appendix I:

$$\begin{aligned}\Theta_m(s) = &\left\{\prod_{k=1}^{J}(1-2s\lambda_k)^{-\frac{1}{2}}\exp\left\{\frac{s\lambda_k b_{mk}^2}{1-2s\lambda_k}\right\}\right\} \\ &\times\left\{\prod_{k=J+1}^{2L}(1+2s\lambda_k)^{-\frac{1}{2}}\exp\left\{\frac{-s\lambda_k b_{mk}^2}{1+2s\lambda_k}\right\}\right\}.\end{aligned} \tag{41}$$

In this case, each of the $2L$ product factors stems from the MGF of a scaled noncentral Chi-square random variable with one degree of freedom [18]. This observation is consistent with (40), consisting of two weighted sums of independent noncentral Chi-square random variables, where each term in the summation results in a multiplicative factor in (41). As with the MGF direct form, substituting into (34) and (35), the decision error probabilities can be found, and the ZZB follows.

Note that compact form of the MGF in (41) does not require matrix inversion at all possible frequencies, although when evaluating $P_e(\Delta)$, it is necessary to re-compute $\boldsymbol{\Sigma}_m$, $\boldsymbol{R}_m$, and the eigendecomposition in (38) for each value of Δ. Overall, the compact form requires less computation than the direct form, and we use the compact form in our numerical examples in Section IX.

V. ZZB Asymptotic Analysis and Threshold Regions

In this section, we derive asymptotic expressions for the ZZB at both low and high SNRs, and show how SNR thresholds can be found to isolate the low and high SNR regimes. We expand the MGF direct form of (32) in a power series as a function of SNR ξ_b for low SNR, and ξ_b^{-1} for high SNR. The MGF in (32) is a function of $\tilde{\boldsymbol{A}}_m(s)$, k_m, and $\tilde{\boldsymbol{p}}_m$. These quantities depend on $\boldsymbol{\Psi}$, that in turn depends on $\boldsymbol{W}$ in (15), where $\boldsymbol{W}$ incorporates $\boldsymbol{X}^{-1}$, and finally $\boldsymbol{X}$ in (13) is a function of the desired expansion variable ξ_b. So, we begin by expanding $\boldsymbol{X}$ in ξ_b, or $\boldsymbol{X}^{-1}$ in ξ_b^{-1}, and then substitute these until we obtain the desired expansion of the MGF.[2]

A. Low SNR Regime

Using the results from Appendix I-B, we find a Taylor expansion of $\boldsymbol{X}^{-1}$ given by

$$\boldsymbol{X}^{-1} = \left(\boldsymbol{I} + \xi_b\boldsymbol{V}^{\frac{1}{2}}\boldsymbol{S}_{00}\boldsymbol{V}^{\frac{1}{2}}\right)^{-1} = \boldsymbol{I} - \xi_b\boldsymbol{V}^{\frac{1}{2}}\boldsymbol{S}_{00}\boldsymbol{V}^{\frac{1}{2}} + \boldsymbol{O}\left(\xi_b^2\right). \tag{42}$$

[2]A similar approach can be applied beginning with the MGF compact form. Along with some common terms arising in the MGF direct form expansion, this also requires expansion of eigendecomposition components $\boldsymbol{P}_m$ and λ_k in (38) that can be obtained using a perturbation technique detailed in [19].

It follows that we can expand $\boldsymbol{V}^{1/2}\boldsymbol{X}^{-1}\boldsymbol{V}^{1/2}$, contained in $\boldsymbol{W}$, as

$$\boldsymbol{V}^{\frac{1}{2}}\boldsymbol{X}^{-1}\boldsymbol{V}^{\frac{1}{2}} = \boldsymbol{V} - \xi_b \boldsymbol{V}\boldsymbol{S}_{00}\boldsymbol{V} + \boldsymbol{O}\left(\xi_b^2\right). \tag{43}$$

Subsequently, $\boldsymbol{\Psi}$ and $\boldsymbol{g}$ become

$$\begin{aligned}\boldsymbol{\Psi} &= \frac{\xi_b^2}{E_{\rm rx}}\boldsymbol{\Psi}_2 + \boldsymbol{O}(\xi_b^3), \quad \boldsymbol{g} = \frac{\xi_b}{\sqrt{E_{\rm rx}}}\boldsymbol{g}_1 + \boldsymbol{O}(\xi_b^2),\\ \boldsymbol{\Psi}_2 &= \begin{bmatrix} \frac{\boldsymbol{V}}{2} & \boldsymbol{0} \\ \boldsymbol{0} & -\frac{\boldsymbol{V}}{2}\end{bmatrix}, \quad \boldsymbol{g}_1 = \begin{bmatrix}\boldsymbol{\mu}_\alpha \\ -\boldsymbol{\mu}_\alpha\end{bmatrix}.\end{aligned} \tag{44}$$

Then, $\tilde{\boldsymbol{A}}_m(s)$, $\tilde{\boldsymbol{p}}_m$ and k_m become

$$\begin{aligned}\tilde{\boldsymbol{A}}_m(s) &= \boldsymbol{I} - 2s\boldsymbol{\Sigma}_m\boldsymbol{\Psi}\\ &= \boldsymbol{I} - 2sE_{\rm rx}\left(\boldsymbol{R}_m\boldsymbol{V}\boldsymbol{R}_m^T + \xi_b^{-1}\boldsymbol{\Gamma}\right)\boldsymbol{\Psi}\\ &= \boldsymbol{I} - 2s\boldsymbol{\Gamma}\boldsymbol{\Psi}_2\xi_b + \boldsymbol{O}\left(\xi_b^2\right), \qquad (45)\\ \tilde{\boldsymbol{p}}_m &= \boldsymbol{g} + 2\boldsymbol{\Psi}\boldsymbol{\mu}_m = \frac{\xi_b}{\sqrt{E_{\rm rx}}}\boldsymbol{g}_1 + \boldsymbol{O}\left(\xi_b^2\right),\\ k_m &= \boldsymbol{\mu}_m^T\boldsymbol{\Psi}\boldsymbol{\mu}_m + \boldsymbol{g}^T\boldsymbol{\mu}_m = \boldsymbol{g}_1^T\boldsymbol{m}_m\xi_b + O\left(\xi_b^2\right). \qquad (46)\end{aligned}$$

Using the Taylor expansions in (108), (109) and (110) in Appendix I-B, the inverse and determinant of $\tilde{\boldsymbol{A}}_m(s)$ can be expanded as

$$\begin{aligned}\tilde{\boldsymbol{A}}_m^{-1}(s) &= \boldsymbol{I} + 2s\xi_b\boldsymbol{\Gamma}\boldsymbol{\Psi}_2 + \boldsymbol{O}\left(\xi_b^2\right)\\ |\tilde{\boldsymbol{A}}_m(s)| &= 1 - 2s\xi_b\mathrm{tr}(\boldsymbol{\Gamma}\boldsymbol{\Psi}_2) + O\left(\xi_b^2\right)\\ |\tilde{\boldsymbol{A}}_m(s)|^{-\frac{1}{2}} &= 1 + s\xi_b\mathrm{tr}(\boldsymbol{\Gamma}\boldsymbol{\Psi}_2) + O\left(\xi_b^2\right).\end{aligned} \tag{47}$$

From (46) and (47), we obtain

$$\tilde{\boldsymbol{p}}_m^T\tilde{\boldsymbol{A}}_m^{-1}(s)\boldsymbol{\Sigma}_m\tilde{\boldsymbol{p}}_m = \xi_b\boldsymbol{g}_1^T\boldsymbol{\Gamma}\boldsymbol{g}_1 + O\left(\xi_b^2\right). \tag{48}$$

Substituting (46) and (47) into (32), the MGF expansion is

$$\begin{aligned}\Theta_m(s) = &\left\{1 + s\xi_b\mathrm{tr}(\boldsymbol{\Gamma}\boldsymbol{\Psi}_2) + O\left(\xi_b^2\right)\right\}\\ &\times\exp\left\{s\xi_b\boldsymbol{g}_1^T\boldsymbol{m}_m + \frac{s^2}{2}\xi_b\boldsymbol{g}_1^T\boldsymbol{\Gamma}\boldsymbol{g}_1 + O\left(\xi_b^2\right)\right\}.\end{aligned} \tag{49}$$

As $\xi_b \to 0$, the leading coefficient in (49) goes to unity, and the first order approximation of the MGF in the low SNR regime is

$$\Theta_m(s) \approx \exp\left\{s\xi_b\boldsymbol{g}_1^T\boldsymbol{m}_m + \frac{s^2}{2}\xi_b\boldsymbol{g}_1^T\boldsymbol{\Gamma}\boldsymbol{g}_1\right\}. \tag{50}$$

This is the MGF of a normally distributed random variable with mean $\xi_b\boldsymbol{g}_1^T\boldsymbol{m}_m$ and variance $\xi_b\boldsymbol{g}_1^T\boldsymbol{\Gamma}\boldsymbol{g}_1$. Thus, at low SNR, $\mathcal{L}_m \sim \mathcal{N}(\xi_b\boldsymbol{g}_1^T\boldsymbol{m}_m, \xi_b\boldsymbol{g}_1^T\boldsymbol{\Gamma}\boldsymbol{g}_1)$. Therefore, (34) and (35) are

$$\begin{aligned}\Pr\{\mathcal{L}_0 < 0\} &= Q\left(\frac{\xi_b\boldsymbol{g}_1^T\boldsymbol{m}_0}{\sqrt{\xi_b\boldsymbol{g}_1^T\boldsymbol{\Gamma}\boldsymbol{g}_1}}\right)\\ \Pr\{\mathcal{L}_1 > 0\} &= Q\left(-\frac{\xi_b\boldsymbol{g}_1^T\boldsymbol{m}_1}{\sqrt{\xi_b\boldsymbol{g}_1^T\boldsymbol{\Gamma}\boldsymbol{g}_1}}\right)\end{aligned} \tag{51}$$

where $Q(x) = (1/\sqrt{2\pi})\int_x^\infty \exp(-t^2/2)dt$ is the Q-function. Substituting (51) into (20) and using the following expansion of the Q-function for small x [16]

$$Q(x) = \frac{1}{2} - \frac{1}{\sqrt{\pi}}\sum_{n=0}^{\infty}\frac{(-1)^n\left(\frac{x}{\sqrt{2}}\right)^{2n+1}}{(2n+1)n!},$$

equation (20) becomes

$$P_e(\Delta) \approx \frac{1}{2} - \frac{1}{2}\frac{\sqrt{\xi_b}\boldsymbol{g}_1^T(\boldsymbol{m}_0 - \boldsymbol{m}_1)}{\sqrt{\pi\boldsymbol{g}_1^T\boldsymbol{\Gamma}\boldsymbol{g}_1}}. \tag{52}$$

Substituting into (6), the low SNR ZZB is approximately

$$\overline{\epsilon^2} \geq \frac{1}{T}\int_0^T \Delta(T-\Delta)\left[\frac{1}{2} - \frac{1}{2}\frac{\sqrt{\xi_b}\boldsymbol{g}_1^T(\boldsymbol{m}_0 - \boldsymbol{m}_1)}{\sqrt{\pi\boldsymbol{g}_1^T\boldsymbol{\Gamma}\boldsymbol{g}_1}}\right]d\Delta. \tag{53}$$

Using the definitions of $\boldsymbol{g}_1$ in (44), $\boldsymbol{\Gamma}$ in (28), $\boldsymbol{R}_m$ in (25) and (26), and $\boldsymbol{m}_m$ in (27), it can be easily shown that

$$\begin{aligned}\boldsymbol{g}_1^T(\boldsymbol{m}_0 - \boldsymbol{m}_1) &= \boldsymbol{g}_1^T\boldsymbol{\Gamma}\boldsymbol{g}_1 = 2\boldsymbol{\mu}_\alpha^T(\boldsymbol{S}_{00} - \boldsymbol{S}_{01})\boldsymbol{\mu}_\alpha\\ &= \sum_{k=-(L-1)}^{L-1} 2\left(\beta_{-kT_t} - \beta_{\Delta-kT_t}\right)\boldsymbol{\mu}_\alpha^T\boldsymbol{J}^k\boldsymbol{\mu}_\alpha.\end{aligned}$$

Therefore, we arrive at the desired low SNR ZZB, given by

$$\begin{aligned}\overline{\epsilon^2} \geq &\frac{1}{T}\int_0^T \Delta(T-\Delta)\\ &\times\left[\frac{1}{2} - \sqrt{\frac{\xi_b}{2\pi}}\sqrt{\sum_{k=-(L-1)}^{L-1}\left(\beta_{-kT_t} - \beta_{\Delta-kT_t}\right)\boldsymbol{\mu}_\alpha^T\boldsymbol{J}^k\boldsymbol{\mu}_\alpha}\right]d\Delta.\end{aligned} \tag{54}$$

The resulting bound is a function of the channel mean $\boldsymbol{\mu}_\alpha$ and signal correlation β_τ, while not depending on the channel correlation because the term associated with $\boldsymbol{\Psi}_2$ in (49) has been neglected.

B. High SNR Regime

Now we consider large ξ_b. We rewrite (13) as

$$\boldsymbol{X} = \left(\boldsymbol{I} + \boldsymbol{V}^{-\frac{1}{2}}\boldsymbol{S}_{00}^{-1}\boldsymbol{V}^{-\frac{1}{2}}\xi_b^{-1}\right)\left(\xi_b\boldsymbol{V}^{\frac{1}{2}}\boldsymbol{S}_{00}\boldsymbol{V}^{\frac{1}{2}}\right)$$

so that the Taylor expansion of $\boldsymbol{X}^{-1}$ can be expressed as

$$\begin{aligned}\boldsymbol{X}^{-1} = &\boldsymbol{V}^{-\frac{1}{2}}\boldsymbol{S}_{00}^{-1}\boldsymbol{V}^{-\frac{1}{2}}\xi_b^{-1}\\ &-\boldsymbol{V}^{-\frac{1}{2}}\boldsymbol{S}_{00}^{-1}\boldsymbol{V}^{-1}\boldsymbol{S}_{00}^{-1}\boldsymbol{V}^{-\frac{1}{2}}\xi_b^{-2} + \boldsymbol{O}\left(\xi_b^{-3}\right)\end{aligned} \tag{55}$$

and it follows that

$$\boldsymbol{V}^{\frac{1}{2}}\boldsymbol{X}^{-1}\boldsymbol{V}^{\frac{1}{2}} = \boldsymbol{S}_{00}^{-1}\xi_b^{-1} - \boldsymbol{S}_{00}^{-1}\boldsymbol{V}^{-1}\boldsymbol{S}_{00}^{-1}\xi_b^{-2} + \boldsymbol{O}\left(\xi_b^{-3}\right). \tag{56}$$

Subsequently, $\boldsymbol{\Psi}$ and $\boldsymbol{g}$ become[3]

$$\begin{aligned}\boldsymbol{\Psi} &= \frac{1}{E_{\rm rx}}\left[\xi_b\boldsymbol{\Psi}_1 + \xi_b^0\boldsymbol{\Psi}_0 + \boldsymbol{O}(\xi_b^{-1})\right]\\ \boldsymbol{g} &= \frac{1}{\sqrt{E_{\rm rx}}}\left[\xi_b^0\boldsymbol{g}_0 + \boldsymbol{O}(\xi_b^{-1})\right]\end{aligned}$$

[3]For clarity in the expansion in terms of SNR ξ_b, we preserve the notation ξ_b^0, although $\xi_b^0 = 1$.

in which

$$\boldsymbol{\Psi}_1 = \frac{1}{2}\begin{bmatrix} \boldsymbol{S}_{00}^{-1} & \boldsymbol{0} \\ \boldsymbol{0} & -\boldsymbol{S}_{00}^{-1} \end{bmatrix}, \quad \boldsymbol{g}_0 = \begin{bmatrix} \boldsymbol{S}_{00}^{-1}\boldsymbol{V}^{-1}\boldsymbol{\mu}_\alpha \\ -\boldsymbol{S}_{00}^{-1}\boldsymbol{V}^{-1}\boldsymbol{\mu}_\alpha \end{bmatrix},$$
$$\boldsymbol{\Psi}_0 = \frac{1}{2}\begin{bmatrix} -\boldsymbol{S}_{00}^{-1}\boldsymbol{V}^{-1}\boldsymbol{S}_{00}^{-1} & \boldsymbol{0} \\ \boldsymbol{0} & \boldsymbol{S}_{00}^{-1}\boldsymbol{V}^{-1}\boldsymbol{S}_{00}^{-1} \end{bmatrix}. \tag{57}$$

Now $\tilde{\boldsymbol{A}}_m(s)$, $\tilde{\boldsymbol{p}}_m$ and k_m have Taylor expansions

$$\begin{aligned}
\tilde{\boldsymbol{A}}_m(s) &= \boldsymbol{I} - 2s\boldsymbol{\Sigma}_m\boldsymbol{\Psi} \\
&= \boldsymbol{I} - 2s\left(\boldsymbol{R}_m\boldsymbol{V}\boldsymbol{R}_m^T + \xi_b^{-1}\boldsymbol{\Gamma}\right) \\
&\quad \times \left[\xi_b\boldsymbol{\Psi}_1 + \xi_b^0\boldsymbol{\Psi}_0 + \boldsymbol{O}\left(\xi_b^{-1}\right)\right] \\
&= \boldsymbol{I} + \boldsymbol{O}\left(\xi_b^{-1}\right) \\
&\quad + s\left[\underbrace{-2\boldsymbol{R}_m\boldsymbol{V}\boldsymbol{R}_m^T\boldsymbol{\Psi}_1}_{\boldsymbol{A}_1}\xi_b\right. \\
&\qquad \left. + \underbrace{\left(-2\boldsymbol{R}_m\boldsymbol{V}\boldsymbol{R}_m^T\boldsymbol{\Psi}_0 - 2s\boldsymbol{\Gamma}\boldsymbol{\Psi}_1\right)}_{\boldsymbol{A}_0}\xi_b^0\right] \\
&= \boldsymbol{I} + s\left(\boldsymbol{A}_1\xi_b + \boldsymbol{A}_0\xi_b^0\right) + \boldsymbol{O}\left(\xi_b^{-1}\right) \qquad (58) \\
\tilde{\boldsymbol{p}}_m &= \boldsymbol{g} + 2\boldsymbol{\Psi}\boldsymbol{\mu}_m \\
&= \frac{1}{\sqrt{E_{\rm rx}}}\left[\underbrace{2\boldsymbol{\Psi}_1\boldsymbol{m}_m}_{\boldsymbol{p}_1}\xi_b\right. \\
&\qquad \left. + \underbrace{\left(\boldsymbol{g}_0 + 2\boldsymbol{\Psi}_0\boldsymbol{m}_m\right)}_{\boldsymbol{p}_0}\xi_b^0 + \boldsymbol{O}\left(\xi_b^{-1}\right)\right] \\
&= \frac{1}{\sqrt{E_{\rm rx}}}\left[\boldsymbol{p}_1\xi_b + \boldsymbol{p}_0\xi_b^0 + \boldsymbol{O}\left(\xi_b^{-1}\right)\right] \qquad (59) \\
k_m &= \boldsymbol{\mu}_m^T\boldsymbol{\Psi}\boldsymbol{\mu}_m + \boldsymbol{g}^T\boldsymbol{\mu}_m \\
&= \boldsymbol{m}_m^T\boldsymbol{\Psi}_1\boldsymbol{m}_m\xi_b \\
&\quad + \left(\boldsymbol{g}_0^T\boldsymbol{m}_m + \boldsymbol{m}_m^T\boldsymbol{\Psi}_0\boldsymbol{m}_m\right)\xi_b^0 + O\left(\xi_b^{-1}\right) \qquad (60)
\end{aligned}$$

where $\boldsymbol{A}_1$ is singular and $\boldsymbol{A}_0$ is non-singular.

Here we focus on the case of large ξ_b, but note that $|s|$ will vary from small to large. In order to easily evaluate the inverse and determinant of $\tilde{\boldsymbol{A}}_m(s)$ for large ξ_b and small-to-large $|s|$, it is inappropriate to view $s\boldsymbol{A}_1$ as the dominant term in (58) due to the singularity of $\boldsymbol{A}_1$ and possibly small $|s|$. Thus, (58) should not be regarded as a power series in ξ_b alone. Instead, an analytically elegant approach would be to expand the appropriate quantities as a function of both s and ξ_b in order to cope with a large range of $|s|$ and large ξ_b. However, this leads to significant complexity, e.g., using piece-wise approximations for different variable range combinations to complete the integration in the probability evaluation. Fortunately, numerical study reveals that the MGF is very steep around its peak at high SNR (the pdf is much flatter than for the low SNR case). This observation permits us to focus on the small $|s|$ region only. Accordingly, we first express the inverse and determinant of $\tilde{\boldsymbol{A}}_m(s)$ with respect to s using the Taylor expansions (108), (109), and (110) in Appendix I-B, and obtain

$$\begin{aligned}
&\tilde{\boldsymbol{A}}_m^{-1}(s) \\
&\quad = \left[\boldsymbol{I} + s\left(\boldsymbol{A}_1\xi_b + \boldsymbol{A}_0\xi_b^0\right) + \boldsymbol{O}(\xi_b^{-1})\right]^{-1} \\
&\quad = \boldsymbol{I} - s\left(\boldsymbol{A}_1\xi_b + \boldsymbol{A}_0\xi_b^0\right) \\
&\qquad + \boldsymbol{O}(|s|^2) + \boldsymbol{O}\left(\xi_b^{-1}\right) \\
&\quad = \xi_b\underbrace{(-s\boldsymbol{A}_1)}_{\boldsymbol{B}_1} + \xi_b^0\underbrace{(\boldsymbol{I} - s\boldsymbol{A}_0)}_{\boldsymbol{B}_0} \\
&\qquad + \boldsymbol{O}(|s|^2) + \boldsymbol{O}\left(\xi_b^{-1}\right) \\
&\quad = \xi_b\boldsymbol{B}_1 + \boldsymbol{B}_0 + \boldsymbol{O}(|s|^2) + \boldsymbol{O}\left(\xi_b^{-1}\right) \qquad (61) \\
&|\tilde{\boldsymbol{A}}_m(s)| \\
&\quad = \left|\boldsymbol{I} + s\left(\boldsymbol{A}_1\xi_b + \boldsymbol{A}_0\xi_b^0\right) + \boldsymbol{O}\left(\xi_b^{-1}\right)\right| \\
&\quad = 1 + s\cdot tr(\xi_b\boldsymbol{A}_1 + \boldsymbol{A}_0) + O(|s|^2) + O\left(\xi_b^{-1}\right) \qquad (62) \\
&|\tilde{\boldsymbol{A}}_m(s)|^{-\frac{1}{2}} = \xi_b\left[-\frac{s}{2}tr(\boldsymbol{A}_1)\right] + \left[1 - \frac{s}{2}tr(\boldsymbol{A}_0)\right] \\
&\qquad + O(|s|^2) + O\left(\xi_b^{-1}\right). \qquad (63)
\end{aligned}$$

By (59) and (61), it follows that

$$\begin{aligned}
&\tilde{\boldsymbol{p}}_m^T\tilde{\boldsymbol{A}}_m^{-1}(s)\boldsymbol{\Sigma}_m\tilde{\boldsymbol{p}}_m \\
&\quad = \left[\boldsymbol{p}_1\xi_b + \boldsymbol{p}_0\xi_b^0 + \boldsymbol{O}(\xi_b^{-1})\right]^T \\
&\qquad \times \left[\xi_b\boldsymbol{B}_1 + \boldsymbol{B}_0 + \boldsymbol{O}(|s|^2) + \boldsymbol{O}\left(\xi_b^{-1}\right)\right] \\
&\qquad \times \left(\boldsymbol{R}_m\boldsymbol{V}\boldsymbol{R}_m^T + \xi_b^{-1}\boldsymbol{\Gamma}\right) \\
&\qquad \times \left[\boldsymbol{p}_1\xi_b + \boldsymbol{p}_0\xi_b^0 + \boldsymbol{O}\left(\xi_b^{-1}\right)\right] \\
&\quad = \xi_b^3 q_3 + \xi_b^2 q_2 + \xi_b q_1 + q_0 + O(|s|^2) \\
&\qquad + O\left(\xi_b^{-1}\right) \qquad (64)
\end{aligned}$$

where

$$\begin{aligned}
q_3 &= \boldsymbol{p}_1^T\boldsymbol{B}_1\boldsymbol{R}_m\boldsymbol{V}\boldsymbol{R}_m^T\boldsymbol{p}_1, \\
q_2 &= \boldsymbol{p}_1^T\boldsymbol{B}_1\left(\boldsymbol{R}_m\boldsymbol{V}\boldsymbol{R}_m^T\boldsymbol{p}_0 + \boldsymbol{\Gamma}\boldsymbol{p}_1\right) \\
&\quad + \left(\boldsymbol{p}_1^T\boldsymbol{B}_0 + \boldsymbol{p}_0^T\boldsymbol{B}_1\right)\boldsymbol{R}_m\boldsymbol{V}\boldsymbol{R}_m^T\boldsymbol{p}_1, \\
q_1 &= \boldsymbol{p}_1^T\boldsymbol{B}_1\boldsymbol{\Gamma}\boldsymbol{p}_0 + \left(\boldsymbol{p}_1^T\boldsymbol{B}_0 + \boldsymbol{p}_0^T\boldsymbol{B}_1\right)\left(\boldsymbol{R}_m\boldsymbol{V}\boldsymbol{R}_m^T\boldsymbol{p}_0 + \boldsymbol{\Gamma}\boldsymbol{p}_1\right) \\
&\quad + \boldsymbol{p}_0^T\boldsymbol{B}_0\boldsymbol{R}_m\boldsymbol{V}\boldsymbol{R}_m^T\boldsymbol{p}_1, \\
q_0 &= \left(\boldsymbol{p}_1^T\boldsymbol{B}_0 + \boldsymbol{p}_0^T\boldsymbol{B}_1\right)\boldsymbol{\Gamma}\boldsymbol{p}_0 \\
&\quad + \boldsymbol{p}_0^T\boldsymbol{B}_0\left(\boldsymbol{R}_m\boldsymbol{V}\boldsymbol{R}_m^T\boldsymbol{p}_0 + \boldsymbol{\Gamma}\boldsymbol{p}_1\right). \qquad (65)
\end{aligned}$$

Substituting (60), (63) and (64) into (32), the MGF becomes

$$\begin{aligned}
&\Theta_m(s) \\
&\quad = \left\{\xi_b\left[-\frac{s}{2}\mathrm{tr}(\boldsymbol{A}_1)\right] + \left[1 - \frac{s}{2}tr(\boldsymbol{A}_0)\right] + O(|s|^2) + O(\xi_b^{-1})\right\} \\
&\qquad \times \exp\left\{\xi_b^3 q_3 + \xi_b^2 q_2 + \xi_b\left[q_1 + s\left(\boldsymbol{m}_m^T\boldsymbol{\Psi}_1\boldsymbol{m}_m\right)\right]\right. \\
&\qquad\quad \left. + q_0 + O(|s|^2) + O\left(\xi_b^{-1}\right)\right\}. \qquad (66)
\end{aligned}$$

Finally, by ignoring the high order terms of both s and ξ_b we obtain the desired high SNR MGF approximation

$$\Theta_m(s) \approx \left\{\xi_b\left[-\frac{s}{2}tr(\boldsymbol{A}_1)\right]+\left[1-\frac{s}{2}tr(\boldsymbol{A}_0)\right]\right\} \times \exp\left\{\xi_b^3 q_3+\xi_b^2 q_2+\xi_b\left[q_1+s\left(\boldsymbol{m}_m^T\boldsymbol{\Psi}_1\boldsymbol{m}_m\right)\right]+q_0\right\}. \tag{67}$$

Setting $s=j2\pi f$ in (67) and substituting into (34) and (35), the probabilities can be found for $P_e(\Delta)$ in (22).

C. Thresholds and Performance Regions

Our asymptotic analysis results at low and high SNRs are valuable in determining disjoint segments of SNR ξ_b, separated by thresholds, that characterize different performance regions. We define the thresholds as the SNR values where the ZZBs and the asymptotic ZZB approximations differ by $1/2$ [16]. Let us apply this rule to the low SNR regime first based on (54). Taking the limit $\xi_b \to 0$, the convergence level is $(1/12)T^2$. Therefore, we can find the threshold $\xi_b=\delta_1$ that yields half of the convergence level

$$\frac{1}{T}\int_0^T \Delta(T-\Delta)\left[\frac{1}{2}-\sqrt{\frac{\delta_1}{2\pi}} \times\sqrt{\sum_{k=-(L-1)}^{L-1}\left(\beta_{-kT_t}-\beta_{\Delta-kT_t}\right)\boldsymbol{\mu}_\alpha^T\boldsymbol{J}^k\boldsymbol{\mu}_\alpha}\right]d\Delta=\frac{1}{24}T^2. \tag{68}$$

Solving this equation numerically, one can obtain δ_1.

The threshold $\xi_b=\delta_2$ at high SNR can be found similarly. Substituting (67) into (34) and (35), and subsequently into (22), $P_e(\Delta)$ follows. Using that result in (6) and setting it equal to half the general ZZB from (6), an equation in δ_2 results.

VI. Important ZZB Special Cases

In this section, we consider the ZZB for three cases of broad interest. First we look at narrowband channels, corresponding to Rayleigh/Ricean flat fading, and we recover a result derived differently by Kozick and Sadler [12], [13]. We then consider wideband channels with independent taps, with the signal bandwidth matching the channel bandwidth. Finally, we consider the deterministic case when the receiver knows the channel.

A. Single Tap Channel

With $L=1$, the channel gain α follows $\mathcal{N}\sim(\mu_\alpha,\sigma_\alpha^2)$ corresponding to Rayleigh/Ricean flat fading. The received signal is modeled by

$$y(t)=\sqrt{E_{\rm rx}}\alpha s_m(t)+n(t), \tag{69}$$

and correlation and other terms are

$$I_y \triangleq \int_{T_0} y^2(t)dt,\ r_m \triangleq \int_{T_0} s_m y(t)dt,$$

$$S_{mm} \triangleq \int_{T_0} s_m^2(t)dt,\ S_{01}=S_{10}\triangleq\int_{T_0} s_0(t)s_1(t)dt,$$

$$X=1+\xi_b\sigma_\alpha^2 S_{00},\ v_m=\frac{\sqrt{E_{\rm rx}}}{\sigma_n^2}\sigma_\alpha r_m-\frac{E_{\rm rx}}{\sigma_n^2}\sigma_\alpha S_{00}\mu_\alpha,$$

$$c_m=\frac{\sqrt{E_{\rm rx}}}{\sigma_n^2}\mu_\alpha r_m-\frac{E_{\rm rx}}{2\sigma_n^2}\mu_\alpha^2 S_{00}-\frac{I_y}{2\sigma_n^2}.$$

The distribution of the received signal is proportional to

$$p(y(t)\,|\,m\Delta)\propto\exp\left\{Wr_m^2+hr_m\right\} \tag{70}$$

where

$$W=\frac{\xi_b^2\sigma_\alpha^2}{2(1+\xi_b\sigma_\alpha^2 S_{00})}$$

$$h=\left[\xi_b-\frac{\xi_b^2\sigma_\alpha^2 S_{00}}{1+\xi_b\sigma_\alpha^2 S_{00}}\right]\mu_\alpha.$$

The mean and variance for $\tilde{\boldsymbol{r}}_m$ are given by

$$\boldsymbol{\mu}_0=\sqrt{E_{\rm rx}}\begin{bmatrix}S_{00}\mu_\alpha\\ S_{10}\mu_\alpha\end{bmatrix},\quad \boldsymbol{\mu}_1=\sqrt{E_{\rm rx}}\begin{bmatrix}S_{01}\mu_\alpha\\ S_{00}\mu_\alpha\end{bmatrix}$$

$$\boldsymbol{\Sigma}_0=E_{\rm rx}\begin{bmatrix}S_{00}^2+\xi_b^{-1}S_{00} & S_{00}S_{10}+\xi_b^{-1}S_{01}\\ S_{00}S_{10}+\xi_b^{-1}S_{10} & S_{10}^2+\xi_b^{-1}S_{00}\end{bmatrix}$$

$$\boldsymbol{\Sigma}_1=E_{\rm rx}\begin{bmatrix}S_{01}^2+\xi_b^{-1}S_{00} & S_{00}S_{01}+\xi_b^{-1}S_{01}\\ S_{00}S_{01}+\xi_b^{-1}S_{10} & S_{00}^2+\xi_b^{-1}S_{00}\end{bmatrix}.$$

In this case, the log-likelihood ratio becomes

$$\mathcal{L}=W\left(r_0^2-r_1^2\right)+h(r_0-r_1)=\boldsymbol{r}^T\boldsymbol{\Psi}\boldsymbol{r}+\boldsymbol{g}^T\boldsymbol{r},$$

$$\boldsymbol{\Psi}=\begin{bmatrix}W & 0\\ 0 & -W\end{bmatrix},\quad \boldsymbol{g}=\begin{bmatrix}h\\ -h\end{bmatrix}. \tag{71}$$

In particular for the Rayleigh fading case $\mu_\alpha=0$, then $h=0$ and $\mathcal{L}=W(r_0^2-r_1^2)$. Since $W>0$, the LLR test reduces to comparison of r_0^2 with r_1^2, the signal power.[4] Thus, the error probability expression before simplification matches (113) in [13] under $N=1$ therein. Moreover, $\boldsymbol{\mu}_0=[0,0]^T$, and

$$\boldsymbol{\Sigma}_0=E_{\rm rx}\xi_b^{-1}\begin{bmatrix}S_{00}+\xi_b S_{00}^2 & (1+\xi_b S_{00})S_{01}\\ (1+\xi_b S_{00})S_{01} & S_{00}+\xi_b S_{10}^2\end{bmatrix} =S_{00}\sigma_n^2(1+\xi_b S_{00})\begin{bmatrix}1 & \frac{S_{01}}{S_{00}}\\ \frac{S_{01}}{S_{00}} & \frac{1+\xi_b\left(\frac{S_{01}^2}{S_{00}}\right)}{1+\xi_b S_{00}}\end{bmatrix}. \tag{72}$$

If we define the SNR as in (75) in [13],

$$\overline{\rm SNR}\triangleq\xi_b,\quad \rho(0)\triangleq S_{00},\quad \rho(\theta)\triangleq S_{01},\quad \mathcal{N}_o\triangleq\sigma_n^2 \tag{73}$$

then our (72) above becomes

$$\boldsymbol{\Sigma}_0=\rho_0\mathcal{N}_0(1+\overline{\rm SNR}\rho_0)\begin{bmatrix}1 & \frac{\rho(\theta)}{\rho_0}\\ \frac{\rho(\theta)}{\rho_0} & \frac{1+\overline{\rm SNR}\left(\frac{\rho(\theta)^2}{\rho_0}\right)}{1+\overline{\rm SNR}\rho_0}\end{bmatrix} \tag{74}$$

[4]As pointed out in [12], [13], the optimal detector corresponds to a non-coherent matched filter.

which takes the same form as (115) in [13]. With the above results, the same closed form expression for error probability P_e as in (116) and (117) of [13] can be obtained as

$$P_e = \frac{1}{2} - \frac{1}{2}\left[1 + \frac{4(1+\overline{\mathrm{SNR}}\cdot\rho(0))}{(\rho(0)\cdot\overline{\mathrm{SNR}})^2\cdot[1-|\rho(\theta)/\rho(0)|^2]}\right]^{-1/2}. \quad (75)$$

See [12], [13] for extension to multiple narrowband independent channels, and further results including CRBs and estimation.

B. Wideband Waveform With Independent Channel Taps

For this case, we assume that the waveform bandwidth matches the channel, with an ideal correlation function such that $\beta_\tau = 0$ for $\tau > T_t$ and $\beta_\tau \neq 0$ for $|\tau| \leq T_t$. Thus, the waveform autocorrelation matrix $\boldsymbol{S}_{00}$ in (10) becomes $\beta_0\boldsymbol{I}$, and $\boldsymbol{S}_{01}$ has at most two nonzero subdiagonals. We also assume independent channel taps, where each channel tap may have different mean and variance. This corresponds to many measured wireless fading channel models, e.g., with an exponential decay in the variance. Now, the channel mean vector is $\boldsymbol{\mu}_\alpha = [\mu_{\alpha_1},\ldots,\mu_{\alpha_L}]^T$ and covariance matrix $\boldsymbol{V} = \mathrm{diag}[\sigma^2_{\alpha_1},\ldots,\sigma^2_{\alpha_L}]$.

Let us examine the dependence of the two data vectors $\boldsymbol{r}_0$ and $\boldsymbol{r}_1$ in the LLR expression. As an example, assume hypothesis H_0. Using (23) and (24), we find

$$\begin{aligned}\mathrm{VAR}(\boldsymbol{r}_0\,|\,H_0) &= E_{\mathrm{rx}}\beta_0^2\boldsymbol{V} + \sigma_n^2\boldsymbol{I}\\ \mathrm{VAR}(\boldsymbol{r}_1\,|\,H_0) &= E_{\mathrm{rx}}\boldsymbol{S}_{10}\boldsymbol{V}\boldsymbol{S}_{10}^T + \sigma_n^2\boldsymbol{I}\\ \mathrm{COV}(\boldsymbol{r}_0|H_0,\boldsymbol{r}_1|H_0) &= E_{\mathrm{rx}}\beta_0\boldsymbol{V}\boldsymbol{S}_{10}^T + \sigma_n^2\boldsymbol{S}_{10}^T. \end{aligned} \quad (76)$$

These simplified expressions can be used to replace their counterparts in our earlier ZZB development.

Remark: Further simplifications do not appear to be straightforward. For example, with multiple independent flat fading (single tap) channels, a simplified ZZB expression is obtained in [13, Sec. 5.3], using results from Appendix B of [4] or Appendix 9A of [5]. However, in our case, note that $\boldsymbol{S}_{10}$ is a function of the continuous variable Δ. While the elements of $\boldsymbol{r}_0$ are independent, the entries of $\boldsymbol{r}_1$ are not necessarily independent except for some special values of Δ such that $\boldsymbol{S}_{10}$ has only one non-zero subdiagonal. Also, from the above covariance, $\boldsymbol{r}_0$ and $\boldsymbol{r}_1$ are generally correlated for most values of Δ. These conditions violate the assumptions used in [13].

C. Known Channel

Next we consider the case when the channel $\boldsymbol{\alpha}$ is fixed and known to the receiver. Now, the LLR is governed by (8), rather than taking the expectation over channel realizations as in (11). The LLR can be easily shown to be $\boldsymbol{r}_0^T\boldsymbol{\alpha} - \boldsymbol{r}_1^T\boldsymbol{\alpha}$, with some constants suppressed.[5] It follows that

$$\mathcal{L}_0 = \sqrt{E_{\mathrm{rx}}}\boldsymbol{\alpha}^T(\boldsymbol{S}_{00}-\boldsymbol{S}_{10})\boldsymbol{\alpha} + \boldsymbol{\alpha}^T(\boldsymbol{z}_0-\boldsymbol{z}_1) \underset{H_1}{\overset{H_0}{\gtrless}} 0$$

[5]With the signal and channel known to the receiver, the corresponding optimal detector is a coherent matched filter.

TABLE I
SYMBOLS AND EQUATIONS FOR EVALUATING THE ZZB AND ITS APPROXIMATIONS

		Notation	Equations
(0) Initialization		T, β_τ, $\boldsymbol{\mu}_\alpha$, $\boldsymbol{V}$, L, T_t	
(1) Intermediate Variables		$\boldsymbol{S}_{00}$, $\boldsymbol{S}_{01}$, $\boldsymbol{S}_{10}$, $\boldsymbol{S}_{11}$	(10)
		$\boldsymbol{R}_0$	(25)
		$\boldsymbol{R}_1$	(26)
		$\boldsymbol{X}$	(13)
		$\boldsymbol{W}$	(15)
		$\boldsymbol{h}$	(16)
		$\boldsymbol{\Psi}$, $\boldsymbol{g}$	(19)
		$\boldsymbol{\Gamma}$	(28)
		$\boldsymbol{\mu}_m$, $\boldsymbol{m}_m$, $\boldsymbol{\Sigma}_m$	(27)
(2) MGF Associated Variables	Direct Form	$\widetilde{\boldsymbol{A}}_m(s)$, k_m, $\widetilde{\boldsymbol{p}}_m$	(33)
	Compact Form	$\boldsymbol{b}_m$	(37)
		λ_k	(38)
	Low SNR Approx.	$\boldsymbol{g}_1$	(44)
	High SNR Approx.	$\boldsymbol{A}_0$, $\boldsymbol{A}_1$	(58)
		q_0, q_1, q_2, q_3	(65)
		$\boldsymbol{\Psi}_0$, $\boldsymbol{\Psi}_1$	(57)
MGF	Direct Form	$\Theta_m(s)$	(32)
	Compact Form		(41)
	Low SNR Approx.		(50)
	High SNR Approx.		(67)
(3) Probability of Error		P_e	(22) (34) (35)
(4) ZZB		$\overline{\epsilon^2}$	(6)

which is Gaussian distributed with mean $\sqrt{E_{\mathrm{rx}}}\boldsymbol{\alpha}^T(\boldsymbol{S}_{00}-\boldsymbol{S}_{10})\boldsymbol{\alpha}$ and variance $\sigma_n^2[\boldsymbol{\alpha}^T(\boldsymbol{s}_0-\boldsymbol{s}_1)]^2$. Then,

$$\Pr\{\mathcal{L}_0<0\} = Q\left(\frac{\sqrt{E_{\mathrm{rx}}}\boldsymbol{\alpha}^T(\boldsymbol{S}_{00}-\boldsymbol{S}_{10})\boldsymbol{\alpha}}{\sigma_n|\boldsymbol{\alpha}^T(\boldsymbol{s}_0-\boldsymbol{s}_1)|}\right).$$

Similarly, it follows that $\Pr\{\mathcal{L}_1>0\}$ takes the same expression as above. Therefore,

$$P_e(\Delta) = \Pr\{\mathcal{L}_0<0\} = Q\left(\frac{\sqrt{\xi_b}\boldsymbol{\alpha}^T(\boldsymbol{S}_{00}-\boldsymbol{S}_{10})\boldsymbol{\alpha}}{|\boldsymbol{\alpha}^T(\boldsymbol{s}_0-\boldsymbol{s}_1)|}\right). \quad (77)$$

Notice that $\boldsymbol{S}_{10}$ and $\boldsymbol{s}_1$ are functions of Δ. Substituting into (6), the ZZB can be evaluated. We can also find the low and high SNR asymptotic ZZB expressions by incorporating the power series expansion of the Q-function in [16], as we did in Section V.

VII. SUMMARY OF THE ZZB COMPUTATION

In this section, we summarize the computation of the ZZB. The ZZB can be evaluated for the various cases as follows, with reference to Table I. The computation flows downward in the table. Below we describe the general ZZB computation, as well as the low and high SNR approximations from Section V. See also Section VI for other special cases.

Step 0 (Initialization): The input parameters to the bound are given as follows. The uniform prior on the time delay is specified by duration T, the signal is specified by its deterministic autocorrelation β_τ, and the random Gaussian channel parameters are mean $\boldsymbol{\mu}_\alpha$, covariance matrix $\boldsymbol{V}$, number of taps L, and the tap spacing in time T_t.

Step 1 (Intermediate variables): Using the initial specification from Step 0, simple linear algebraic operations yield the intermediate variables $\boldsymbol{S}_{00}$, $\boldsymbol{S}_{01}$, $\boldsymbol{S}_{10}$, $\boldsymbol{S}_{11}$, $\boldsymbol{R}_0$, $\boldsymbol{R}_1$, $\boldsymbol{X}$, $\boldsymbol{W}$, $\boldsymbol{h}$, $\boldsymbol{\Psi}$, $\boldsymbol{g}$, $\boldsymbol{\Gamma}$, and the distribution parameters $\boldsymbol{\mu}_m$, $\boldsymbol{m}_m$ and $\boldsymbol{\Sigma}_m$ of the data vector $\boldsymbol{r}_m$.

Step 2 (Moment generating function). Next the MGF is calculated. Generally, either the direct form or the compact form can be employed (see the discussion in Section IV). In the table, we also show the variables associated with the low and high SNR asymptotic cases.

1) *MGF direct form*: The variables $\tilde{\boldsymbol{A}}_m(s)$, k_m and $\tilde{\boldsymbol{p}}_m$ are calculated, and then the MGF is computed by (32).
2) *MGF compact form*: The variable $\boldsymbol{b}_m$ is found by (37), and the eigenvalues λ_k of $\boldsymbol{\Sigma}_m^{1/2}\boldsymbol{\Psi}\boldsymbol{\Sigma}_m^{1/2}$ using (38). The MGF is computed by substitution into (41).
3) *Low SNR approximation*: Compute $\boldsymbol{g}_1$ from (44), and then use (50).
4) *High SNR approximation*: Compute variables $\boldsymbol{A}_0$, $\boldsymbol{A}_1$, q_0, q_1, q_2, q_3, $\boldsymbol{\Psi}_0$, and $\boldsymbol{\Psi}_1$, and then use (67).

Step 3 (Probability of error): Next P_e, the probability of error of the hypothesis test associated with the ZZB, is found by substituting the MGF from Step 2 into (34) and (35), and then into (22). Note that for the low SNR approximation, P_e can alternatively be computed using (52).

Step 4. The ZZB is obtained by substituting P_e into (6).

Next we discuss numerical issues in the ZZB computation relating to the MGF. The MGF can be computed using the direct or the compact form. The direct form relies on computing the determinant and inverse of $\tilde{\boldsymbol{A}}_m(s)$ for each $s = j2\pi f$, which is computationally expensive. The compact form allows us to exploit the symmetry of $\boldsymbol{\Sigma}_m^{1/2}\boldsymbol{\Psi}\boldsymbol{\Sigma}_m^{1/2}$ to compute the determinant and inverse efficiently from its eigenvalues and eigenvectors, which are independent of s, and then (41) follows easily. Thus, the compact form is generally preferred, and we adopt it in our numerical studies that follow.

Step 3 relies on the Fourier transform of the MGF in (34) and (35), which can be computed efficiently using the FFT, but requires truncation in the frequency variable f due to the infinite integration limits. Thus, the truncation value must be specified, as well as the size of the FFT used to sample the MGF up to its truncation point. As we noted in Section V, the MGF concentrates around its peak at high SNR, and in the cases we have studied, the truncation error diminishes rapidly. However, at lower SNR, larger truncation thresholds are generally required, and longer FFTs are needed to sample the truncated MGF.

A related issue, arising with the MGF transform computation, is the inherent rectangular window weighting; the pdf estimate is convolved with a sinc function. When P_e is large (i.e., low SNR), any numerically induced error is generally negligible. But when P_e is small (high SNR), then oscillations in the pdf estimate may lead to an error in P_e. Therefore, generally at high SNR, we smooth the pdf estimate by convolving with a positive valued smoothing function, ensuring that the pdf estimate is strictly greater than or equal to zero. The appropriate length of the averaging window depends on the sampling interval of the pdf. The oscillation can also be alleviated by increasing the MGF truncation window length as well as the FFT length within the window, with an increase in computational complexity.

VIII. Bayesian TDE Estimation, the Average Conditional CRB, and the ZZB

For comparison with our ZZB, we first present the MAP and Bayesian maximum likelihood (ML) time delay estimators. Then we develop an alternative bound, deriving the expected value of the conditional CRB, averaging over the random channel. Finally, we compare the MAP estimator mean square error performance at low SNR to that predicted by the ZZB, and show how the approximations in the ZZB lead to a bound that does not precisely converge to the prior distribution at low SNR, whereas the MAP estimator does. Convergence of the MAP estimate to the ZZB at high SNR is shown in the examples in Section IX.

A. Bayesian Time Delay Estimation

The MAP and Bayesian ML estimators are commonly used for estimating random parameters. Generally they are equivalent as the SNR increases to infinity. However, if the *a priori* distribution of the parameter is uniformly distributed, these two estimators are the same in the whole range of SNR [20]. For our case the unconditional distribution of the received signal, averaged over the channel distribution, is given by (14). With the uniform prior on the time delay $f_{t_0}(t_0) = 1/T$, then the MAP and Bayesian ML estimators are

$$\begin{aligned}\hat{t}_{0,\,\mathrm{MAP}} &= \arg\max_{t_0}\{f_{t_0}(t_0)p(y(t)\,|\,t_0)\}\\ &= \arg\max_{t_0}\left\{\frac{1}{T}\exp(\boldsymbol{r}_{t_0}^T\boldsymbol{W}\boldsymbol{r}_{t_0}+\boldsymbol{h}^T\boldsymbol{r}_{t_0})\right\} \qquad (78)\\ \hat{t}_{0,\mathrm{ML}} &= \arg\max_{t_0}\{p(y(t)\,|\,t_0)\}\\ &= \arg\max_{t_0}\left\{\exp\left(\boldsymbol{r}_{t_0}^T\boldsymbol{W}\boldsymbol{r}_{t_0}+\boldsymbol{h}^T\boldsymbol{r}_{t_0}\right)\right\} \qquad (79)\end{aligned}$$

and so they are identical in this case.

For later comparison, we also state the generalized maximum likelihood estimate (GMLE). For our problem, this assumes the channel is deterministic and estimates the time delay by

$$\begin{aligned}\hat{t}_{0,\mathrm{GML}} &= \arg\max_{t_0}\{p(y(t)\,|\,t_0,\boldsymbol{\alpha})\}\\ &= \arg\max_{t_0}\left\{\exp\left[-\frac{1}{2\sigma_n^2}\int_{T_0}\left(y(t)-\sqrt{E_{\mathrm{rx}}}\boldsymbol{\alpha}^T\boldsymbol{s}_{t_0}\right)^2 dt\right]\right\}.\end{aligned} \qquad (80)$$

This GMLE does not use knowledge of the channel distribution, and is then equivalent to a minimum-mean-squared error (MMSE) estimator [21]. In Section IX we will see that lack of knowledge of the channel distribution significantly impairs the performance of the GMLE with respect to MAP estimation.

B. Cramér–Rao Bound

Next we consider the Cramér–Rao bound for our problem. Generally, we should employ the Bayesian CRB (BCRB). However here, with a uniform prior, the regularity condition for computing the BCRB is not satisfied and consequently the BCRB does not exist [17]. As an alternative, we derive the expectation of the CRB conditioned on the random channel, which we refer to as the expected conditional CRB (ECRB) [9].

Generally, if the estimator is assumed asymptotically conditionally unbiased for every value of the random parameter, the MAP/ML estimators should provide performance converging to the ECRB at infinite SNR, as established in [9]. For the time delay estimation problem at hand, the ZZB and MLE are based on the distribution in (14), which has been averaged on the channel distribution, while the ECRB is to be derived from the distribution in (8) which is conditioned on the channel. Thus,

the ECRB may not converge to the prior distribution at low SNR, and at high SNR it may be a slightly weaker bound than the ZZB, as will be demonstrated in our numerical examples in Section IX.

From (8), the log-probability conditioned on the random time delay t_0 and the random channel vector $\boldsymbol{\alpha}$ is given by

$$\ln p(y\,|\,t_0,\boldsymbol{\alpha}) = -\frac{1}{2\sigma_n^2}\int_{T_0}[y(t) - \sqrt{E_{\rm rx}}\boldsymbol{\alpha}^T\boldsymbol{s}(t-t_0)]^2 dt + \ln\mathcal{K}. \quad (81)$$

Differentiating, we have

$$\frac{d\ln p(y\,|\,t_0,\boldsymbol{\alpha})}{dt_0} = -\frac{1}{2\sigma_n^2}\int_{T_0} 2\left[y(t) - \sqrt{E_{\rm rx}}\boldsymbol{\alpha}^T\boldsymbol{s}(t-t_0)\right] \times\left[-\sqrt{E_{\rm rx}}\boldsymbol{\alpha}^T\frac{d\boldsymbol{s}(t-t_0)}{dt_0}\right]dt. \quad (82)$$

Note that the required regularity condition is satisfied

$$E_{y\,|\,t_0,\alpha}\left\{\frac{d\ln p(y\,|\,t_0,\boldsymbol{\alpha})}{dt_0}\right\} = -\frac{1}{2\sigma_n^2}\int_{T_0} 2[E_{y\,|\,t_0,\alpha}\{y(t)\,|\,t_0,\boldsymbol{\alpha}\} - \sqrt{E_{\rm rx}}\boldsymbol{\alpha}^T\boldsymbol{s}(t-t_0)] \times\left[-\sqrt{E_{\rm rx}}\boldsymbol{\alpha}^T\frac{d\boldsymbol{s}(t-t_0)}{dt_0}\right]dt = 0 \quad (83)$$

where

$$E_{y\,|\,t_0,\alpha}\{y(t)\,|\,t_0,\boldsymbol{\alpha}\} = \sqrt{E_{\rm rx}}\boldsymbol{\alpha}^T\boldsymbol{s}(t-t_0). \quad (84)$$

The second derivative is

$$\frac{d^2\ln p(y\,|\,t_0,\boldsymbol{\alpha})}{dt_0^2} = \frac{1}{\sigma_n^2}\int_{T_0}\left\{\sqrt{E_{\rm rx}}y(t)\boldsymbol{\alpha}^T\frac{d^2\boldsymbol{s}(t-t_0)}{dt_0^2} - E_{\rm rx}\frac{d\boldsymbol{s}^T(t-t_0)}{dt_0}\boldsymbol{\alpha}\boldsymbol{\alpha}^T\frac{d\boldsymbol{s}(t-t_0)}{dt_0} - E_{\rm rx}\boldsymbol{s}^T(t-t_0)\boldsymbol{\alpha}\boldsymbol{\alpha}^T\frac{d^2\boldsymbol{s}(t-t_0)}{dt_0^2}\right\}dt. \quad (85)$$

The Fisher information is

$$\begin{aligned} J_F(t_0,\boldsymbol{\alpha}) &= E_{y\,|\,t_0,\alpha}\left\{-\frac{d^2\ln p(y\,|\,t_0,\boldsymbol{\alpha})}{dt_0^2}\right\} \\ &= \xi_b\int_{T_0}\frac{d\boldsymbol{s}^T(t-t_0)}{dt_0}\boldsymbol{\alpha}\boldsymbol{\alpha}^T\frac{d\boldsymbol{s}(t-t_0)}{dt_0}dt \\ &= \xi_b\boldsymbol{\alpha}^T\left[\int_{T_0}\frac{d\boldsymbol{s}(t-t_0)}{dt_0}\frac{d\boldsymbol{s}^T(t-t_0)}{dt_0}dt\right]\boldsymbol{\alpha} \\ &= \xi_b\boldsymbol{\alpha}^T\boldsymbol{\Phi}\boldsymbol{\alpha} = \xi_b\Upsilon(\boldsymbol{\alpha}) \end{aligned} \quad (86)$$

where $\boldsymbol{\Phi} = \int_{T_0}(d\boldsymbol{s}(t-t_0)/dt_0)(d\boldsymbol{s}^T(t-t_0)/dt_0)dt$ and $\Upsilon(\boldsymbol{\alpha}) = \boldsymbol{\alpha}^T\boldsymbol{\Phi}\boldsymbol{\alpha}$.

To compute the ECRB, we compute the inverse of the above Fisher information that is conditioned on both the prior on the time delay and the random channel, and then evaluate its expected value with respect to both quantities

$$\begin{aligned} \text{ECRB} &\triangleq E_{t_0,\alpha}\left\{J_F^{-1}(t_0,\boldsymbol{\alpha})\right\} \\ &= \frac{1}{\xi_b}\int\frac{1}{\boldsymbol{\alpha}^T\boldsymbol{\Phi}\boldsymbol{\alpha}}\cdot p(\boldsymbol{\alpha})d\boldsymbol{\alpha} = \frac{1}{\xi_b}E_\alpha\{\Upsilon^{-1}(\boldsymbol{\alpha})\} \end{aligned} \quad (87)$$

where the distribution of $\boldsymbol{\alpha}$ is multivariate normal with mean $\boldsymbol{\mu}_{\boldsymbol{\alpha}}$ and variance $\boldsymbol{V}$

$$p(\boldsymbol{\alpha}) = \frac{1}{(2\pi)^{L/2}\,|\,\mathbf{V}\,|^{1/2}}\exp\left[-\frac{1}{2}(\boldsymbol{\alpha}-\boldsymbol{\mu}_{\boldsymbol{\alpha}})^T\mathbf{V}^{-1}(\boldsymbol{\alpha}-\boldsymbol{\mu}_{\boldsymbol{\alpha}})\right]. \quad (88)$$

Note that log(ECRB) is linearly decreasing with log(SNR), so the slope of its root mean square equals $-(1/2)$.

Next we evaluate $E_\alpha\{\Upsilon^{-1}(\boldsymbol{\alpha})\}$ in (87). The result of (4.5d.4) in [18] shows the negative power of a quadratic form can be expressed as an integral

$$[\Upsilon(\mathbf{x})]^{-h} = \frac{1}{\Gamma(h)}\int_0^\infty z^{h-1}e^{-z\Upsilon(\mathbf{x})}dz \quad (89)$$

where $\Gamma(h)$ is the Gamma function. Applying this result, we have

$$\begin{aligned} E_\alpha\left\{\Upsilon^{-1}(\boldsymbol{\alpha})\right\} &= E_\alpha\left\{\int_0^\infty e^{-z\Upsilon(\boldsymbol{\alpha})}dz\right\} \\ &= \int_0^\infty E_\alpha\left\{e^{-z\Upsilon(\boldsymbol{\alpha})}\right\}dz \\ &= -\int_{-\infty}^0 E_\alpha\{e^{s\Upsilon(\boldsymbol{\alpha})}\}ds \end{aligned} \quad (90)$$

in which $E_\alpha\{e^{s\Upsilon(\boldsymbol{\alpha})}\}$ is the moment generating function of $\Upsilon(\boldsymbol{\alpha})$. We can use the result of (100) in Appendix I to express it as

$$\begin{aligned} E_\alpha\left\{e^{s\Upsilon(\boldsymbol{\alpha})}\right\} &= \left|\mathbf{I} - 2s\mathbf{V}^{\frac{1}{2}}\boldsymbol{\Phi}\mathbf{V}^{\frac{1}{2}}\right|^{-\frac{1}{2}} \\ &\quad\times\exp\left\{s\boldsymbol{\mu}_\alpha^T\boldsymbol{\Phi}\boldsymbol{\mu}_\alpha + 2s^2\boldsymbol{\mu}_\alpha^T\boldsymbol{\Phi}\mathbf{V}^{\frac{1}{2}}\left(\mathbf{I} - 2s\mathbf{V}^{\frac{1}{2}}\boldsymbol{\Phi}\mathbf{V}^{\frac{1}{2}}\right)^{-1} \times\mathbf{V}^{\frac{1}{2}}\boldsymbol{\Phi}\boldsymbol{\mu}_\alpha\right\}. \end{aligned} \quad (91)$$

This closed form MGF can be computed numerically, and note that a compact form similar to that in Section IV-B can be used to accelerate the computation. The ECRB is then easily obtained from (91), (90), and (87) by numerical integration.

C. Comparing Bayesian TDE and the ZZB at Low SNR

In the low SNR regime, the Bayesian TDE is noise dominated, and the TDE MSE converges to the variance of the prior as the SNR goes to zero. With the uniform prior $f_{\hat{t}_0}(\hat{t}_0) = 1/T$ over $[0,T]$, the MSE of our Bayesian estimate is $\epsilon^2 = (T^2)/(6)$. However, the low SNR convergence level of the ZZB was derived in Section V-C to be $T^2/12 = 1/2\epsilon^2$, so the ZZB does not converge to the prior at low SNR. (For example, see Fig. 2 in the next section.) This occurs because two key inequalities applied throughout the bound development by Ziv and Zakai [7]

are not tight at low SNR. In the following, we explain this gap by computing the bounding errors for our problem.

First, consider the last inequality in (3) of [7], and we obtain

$$\begin{aligned}
&\frac{1}{2}\int_0^{\Delta} \Pr\left\{\epsilon < -\frac{\Delta}{2} \,|\, a\right\} da \\
&\quad = \frac{1}{2}\int_0^{\Delta} \Pr\left\{(\hat{t}_0 - a) < -\frac{\Delta}{2} \,|\, a\right\} da \\
&\quad = \frac{1}{2}\int_0^{\Delta} \Pr\left\{\hat{t}_0 < \left(a - \frac{\Delta}{2}\right) \middle| \, a\right\} da \\
&\quad = \frac{1}{2}\int_{\frac{\Delta}{2}}^{\Delta} \frac{1}{T}\left(a - \frac{\Delta}{2}\right) da \\
&\quad = \frac{1}{2}\cdot\frac{\Delta^2}{8T} \qquad (92)
\end{aligned}$$

$$\begin{aligned}
&\frac{1}{2}\int_{T-\Delta}^{T} \Pr\left\{\epsilon > -\frac{\Delta}{2} \middle| \, a\right\} da \\
&\quad = \frac{1}{2}\int_{T-\Delta}^{T} \Pr\left\{(\hat{t}_0 - a) > \frac{\Delta}{2} \middle| \, a\right\} da \\
&\quad = \frac{1}{2}\int_{T-\Delta}^{T} \Pr\left\{\hat{t}_0 > \left(a + \frac{\Delta}{2}\right) \middle| \, a\right\} da \\
&\quad = \frac{1}{2}\int_{T-\Delta}^{T-\frac{\Delta}{2}} \frac{1}{T}\left[T - \left(a + \frac{\Delta}{2}\right)\right] da \\
&\quad = \frac{1}{2}\cdot\frac{\Delta^2}{8T}. \qquad (93)
\end{aligned}$$

Then the extra error $\overline{\epsilon_{\text{inc1}}^2}$ corresponding to $1/T\int_0^T \Delta\int_0^{T-\Delta} P_e(a, a+\Delta) da d\Delta$ in the same equation is

$$\begin{aligned}
\overline{\epsilon_{\text{inc1}}^2} &= \frac{1}{2}\int_0^T \Delta\left[\frac{1}{T}\int_0^{\Delta} \Pr\left\{\epsilon < -\frac{\Delta}{2}\middle| \, a\right\}\right. \\
&\qquad \left. + \Pr\left\{\epsilon > -\frac{\Delta}{2}\middle| \, a\right\} da\right] d\Delta \\
&= \frac{1}{2}\int_0^T \Delta\left(\frac{1}{T}\frac{\Delta^2}{8T}\times 2\right) d\Delta = \frac{T^2}{32}. \qquad (94)
\end{aligned}$$

The other inequality causing an extra bounding error is from $4\int_0^{T/2} xF(x)dx$ to $4\int_0^T xF(x)dx$ in the derivation above (5) of [7], in which $F(x)$ has the following expression:

$$\begin{aligned}
F(x) &= \frac{1}{T}\int_0^T \Pr\{|\epsilon| \geq x | a\} da \\
&= \frac{1}{T}\int_0^T \Pr\{|\hat{t}_0 - a| \geq x | a\} da \\
&= \frac{1}{T}\int_0^T \Pr\{\hat{t}_0 \geq a + x \text{ or } \hat{t}_0 \leq a - x \,|\, a\} da \\
&= \frac{1}{T}\int_0^{T-x} \Pr\{\hat{t}_0 \geq a + x \,|\, a\} da \\
&\quad + \frac{1}{T}\int_x^T \Pr\{\hat{t}_0 \leq a - x | a\} da \\
&= \frac{1}{T}\int_0^{T-x}\left(\int_{a+x}^T \frac{1}{T} d\hat{t}_0\right) da \\
&\quad + \frac{1}{T}\int_x^T \left(\int_{a+x}^T \frac{1}{T} d\hat{t}_0\right) da \\
&= \left(1 - \frac{x}{T}\right)^2. \qquad (95)
\end{aligned}$$

Then the additional error $\overline{\epsilon_{\text{inc2}}^2}$ corresponding to $(1/T)\int_0^T \Delta\int_0^{T-\Delta} P_e(a, a+\Delta) da d\Delta$ is

$$\begin{aligned}
\overline{\epsilon_{\text{inc2}}^2} &= 2\int_{\frac{T}{2}}^T xF(x)dx = 2\int_{\frac{T}{2}}^T x\left(1 - \frac{x}{T}\right)^2 dx \\
&= \left(\frac{1}{12} - \frac{1}{32}\right)T^2. \qquad (96)
\end{aligned}$$

Finally, during the development in [7] from $(1/T)\int_0^T \Delta\int_0^{T-\Delta} P_e(a, a+\Delta) da d\Delta$ to $\overline{\epsilon^2} = -\int_0^{T+} x^2 dF(x)$, the total extra error is

$$\overline{\epsilon_{\text{inc}}^2} = \overline{\epsilon_{\text{inc1}}^2} + \overline{\epsilon_{\text{inc2}}^2} = \frac{T^2}{32} + \left(\frac{1}{12} - \frac{1}{32}\right)T^2 = \frac{T^2}{12}. \qquad (97)$$

Noting that $T^2/6 - T^2/12 = T^2/12$, this verifies the bound gap between the prior and the ZZB.

IX. Examples

In this section, we present examples of estimation performance and the corresponding bounds. The ZZB evaluation uses the compact form, as described in Section VII. In addition to the ZZB and ECRB developed in this paper, we also plot the "average ZZB" derived in [16]; this version of the ZZB assumes the channel is known to the receiver, and the bound is averaged over the channel statistics. It is interesting to compare the average ZZB to the ZZB developed here, which does not assume knowledge of the channel and so is more realistic for the random channel case.

We plot the root MSE (RMSE) of the TDE as the performance metric. Unless otherwise specified, the signal is a square-root raised cosine (SRRC) pulse (see Appendix II) with roll-off factor $\beta = 0$ and parameter $T_p = 2$. The channel is Gaussian with $T_t = 1$, and $L = 5$ independent taps, and the prior has $T = 30$. Note we normalize time to the channel tap spacing. Based on measured wideband channels [6], an exponential power delay profile is employed with decay factor $\lambda = 6$, the mean of the first tap corresponding to a Ricean-K factor for the first path of $K = 20$ dB, and all other taps with zero mean.

Fig. 1 plots the ZZB and the average ZZB, illustrating the low, medium, and high SNR regions with thresholds. The ZZB and average ZZB are coincident at low SNR, converging to $T/\sqrt{12}$ plotted as a horizontal line. The low SNR approximation from (53) or (54) is shown valid up to 0 dB, and converges to $T/\sqrt{12}$ as the SNR decreases to zero. Using (68) and shifting 3dB down from the convergence MSE level (i.e., 1.5 dB in terms of RMSE), we obtain the low-SNR breakdown point to be $\delta_1 \approx -4.1$ dB as shown in the figure. Beyond δ_1, the ZZB and the average ZZB separate, with a roughly 3 dB loss in RMSE performance due to the lack of channel knowledge that is reflected in the tighter ZZB. The high SNR threshold occurs at $\delta_2 \approx 17.4$ dB. Beyond δ_2, the ZZB and average ZZB both linearly decrease with increasing SNR, with a slope of about

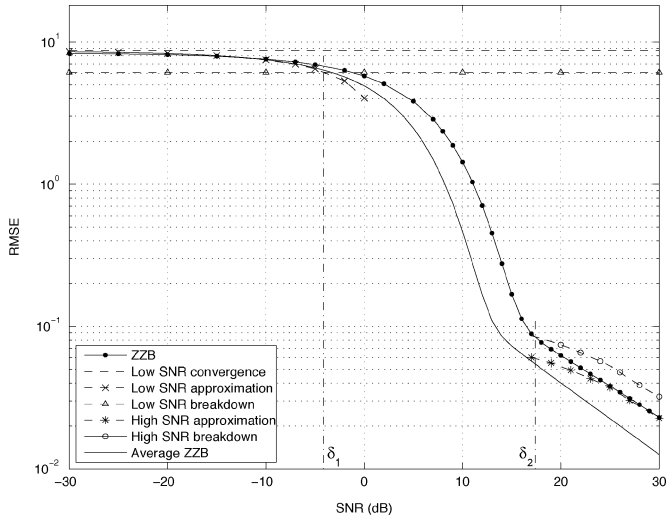

Fig. 1. Typical ZZB behavior for time delay estimation, including low, medium, and high SNR regimes with thresholds δ_1 and δ_2. The channel is Gaussian with strong Ricean K-factor in the first tap, and exponential power decay profile. The average ZZB is a weaker bound that assumes the channel is known to the receiver.

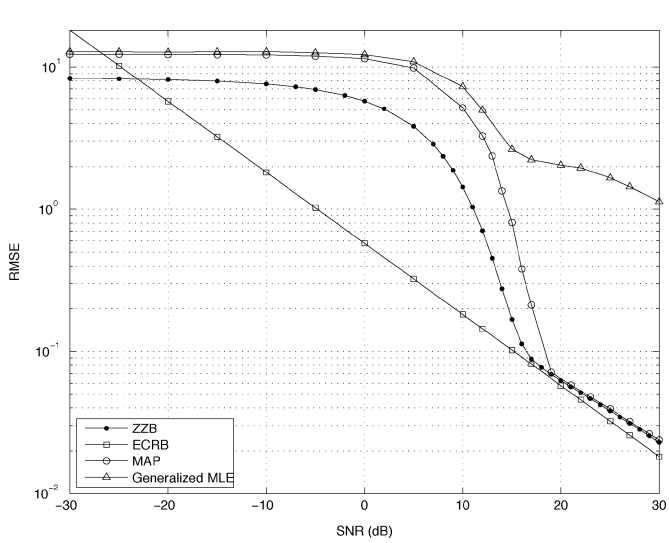

Fig. 2. MAP time delay estimation performance, with ZZB and ECRB comparison. The ZZB tracks the estimator threshold behavior, while the ECRB is not tight below the SNR threshold. The GMLE minimizes the MSE without knowledge of the channel statistics and consequently has much worse performance.

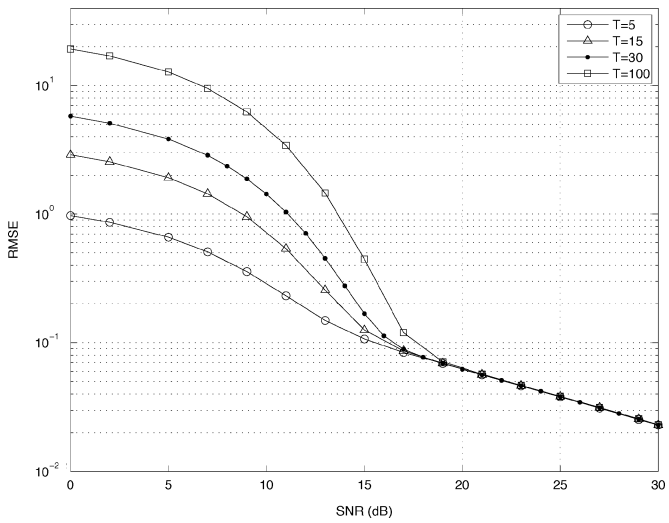

Fig. 3. ZZB on time delay with curves parameterized by prior distribution $[0, T]$, $T = (5, 15, 30, 100)$. The threshold performance improves when T is close to the channel duration LT_t, while the performance is independent of the prior at high SNR.

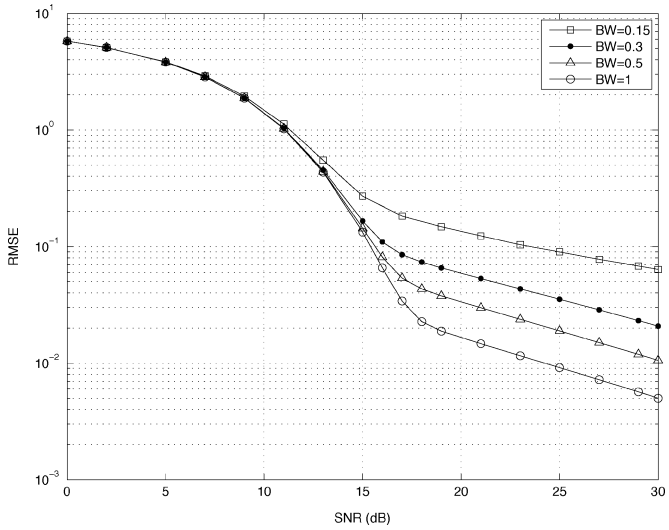

Fig. 4. ZZB on TDE with varying signal bandwidth. A square-root raised cosine pulse with roll-off factor $\beta = 0$ is assumed. Curves are parameterized by the root-mean-square bandwidth for (0.15, 0.3, 0.5, 1). At high SNR, increasing the bandwidth by roughly an order of magnitude decreases the TDE RMSE by an order of magnitude.

-0.5, consistent with bandwidth limited pulse cases studied by Ziv and Zakai [7], [8].

Fig. 2 compares estimators and bounds, averaging over 30 000 realizations. The MAP estimator (78) converges to the ZZB at high SNR, with a few dB gap between the ZZB and MAP estimator in the mid-SNR threshold region, as occurs in frequency estimation and other problems [9]. Also shown is the GMLE from (80), which tracks the MAP performance only at low SNR and generally has weak performance. At high SNR, the ECRB is slightly looser than the ZZB, and because the CRB is a local bound it does not track the MAP threshold behavior and becomes very loose for medium to low SNR.

Fig. 3 plots the ZZB with curves parameterized by the uniform prior distribution duration $[0, T]$, varying T over $T = (5, 15, 20, 100)$. With the prior equal to the channel duration $T = LT_t = 5$, the threshold behavior is enhanced by several decibels. At high SNR, the RMSE performance is independent of the prior.

Next, in Fig. 4, we show the ZZB as a function of signal bandwidth, where we employ the mean-square bandwidth (MSB) defined by (111) in Appendix II. The root-raised cosine pulse was used, with root-MSBs of (0.15, 0.3, 0.5, 1). See Appendix II for the relevant expressions. Increased bandwidth has significant impact above the high SNR threshold, where performance is dominated by the signal autocorrelation and the associated ambiguities [22]. Increasing the root-MSB from 0.15 to 1 yields roughly an order of magnitude reduction in the TDE RMSE in the high SNR regime.

To illustrate the effect of the signal choice we consider several different signals including SRRC, pseudo-random (PN)

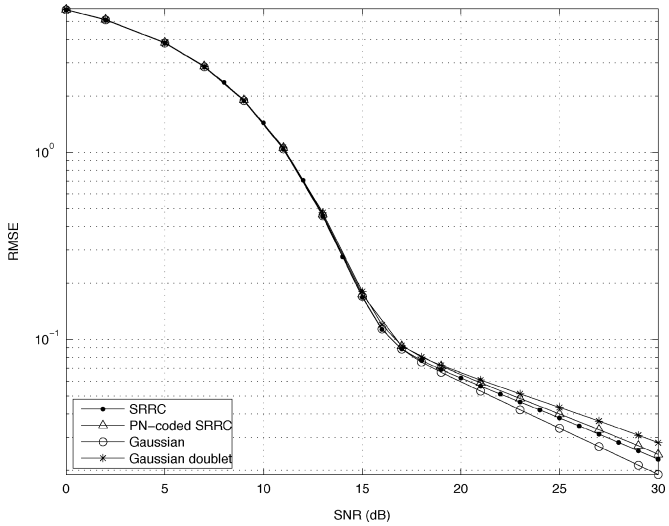

Fig. 5. Ziv–Zakai bounds on time delay, comparing several different signals, all with identical root-mean squared bandwidth. The threshold and low SNR behaviors are identical, while the high SNR performance depends on the detailed structure of the signal autocorrelation.

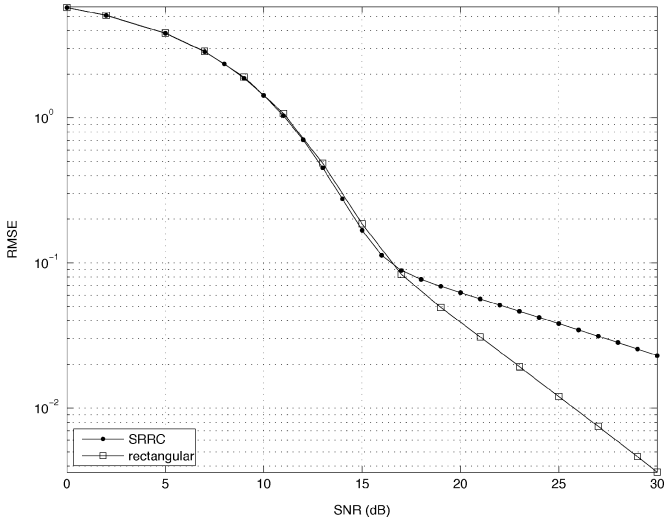

Fig. 6. Ziv–Zakai bounds on time delay, comparing square-root raise cosine (SRRC) and ideal rectangular signals, assuming the main lobe bandwidth of the rectangular signal is same as the SRRC bandwidth of 0.5. The ideal rectangular pulse yields significantly better TDE performance at high SNR due to its broad spectral occupancy compared to the SRRC pulse.

coded SRRC pulse train, Gaussian, and Gaussian doublet in Fig. 5. The root-MSBs were all set to $1/\sqrt{12}$ unit frequency (see Appendix II for the signal and bandwidth expressions). From (27) and (28), the pulse shaping only affects the distributions of the LLR and the ZZB through their autocorrelation matrices $\boldsymbol{S}_{00}$ and $\boldsymbol{S}_{01}$, accounting for the small variation in RMSE error slope in the high SNR regime. Given the same MSB, the threshold and low SNR behaviors are identical.

As a final example, in Fig. 6, we compare a rectangular pulse of duration $T_p = 2$ with the bandlimited SRRC. For comparison, the SRRC bandwidth is set to the width of the rectangular pulse spectrum main lobe, which is $1/T_p$. While these two signals have nominally the same bandwidth, the rectangular pulse yields a TDE RMSE slope of -1 (consistent with [8]) versus $-(1/2)$ for the SRRC. This illustrates the difficulty in selecting a universal definition of bandwidth, without accounting for the rate of spectral decay. The rectangular pulse has much broader spectral shape, and leads to significantly better TDE performance, although the ideal rectangular pulse is not bandlimited and can only be approximated in practice.

X. Conclusion

We developed a Ziv–Zakai bound on Bayesian estimation of time delay, for a known signal propagating through an unknown convolutive random Gaussian channel, with a uniform prior on the delay. The bound does not assume knowledge of the channel at the receiver, providing a tight bound (tighter than a previously derived ZZB that assumes channel knowledge, referred to in this paper as the average ZZB). Differences between the two bounds are pronounced at moderate and high SNRs.

Comparisons with the RMSE performance of MAP estimation indicate that the ZZB is tight for a large range of SNRs, and thresholds can be found that separate low, medium, and high SNR regimes. Lack of precise convergence to the prior as the SNR goes to zero is well known for the ZZB, and this was accounted for by studying the ZZB approximations at low SNR.

The Bayesian CRB is not available with a uniform prior due to regularity (smoothness) violations, so we derived the expectation of the conditional CRB (the ECRB), conditioned on the channel. The ECRB was reasonably tight at high SNR in our examples, but does not capture the threshold TDE behavior and is not tight below the high SNR threshold.

We also considered an MMSE time delay estimator that does not exploit the channel statistics, and showed that the MMSE estimator is considerably poorer than the MAP estimator that does account for the random channel.

Appendix I

A. MGF of a Quadratic Function of a Gaussian Random Vector

Assume $\boldsymbol{r}$ is a real Gaussian vector with distribution $\boldsymbol{r} \sim \mathcal{N}(\boldsymbol{\mu}, \boldsymbol{C})$, where $\boldsymbol{C} > 0$. For constant $\boldsymbol{\Psi}$, $\boldsymbol{g}$ and d, the MGF of $Q = \boldsymbol{r}^T\boldsymbol{\Psi}\boldsymbol{r} + \boldsymbol{g}^T\boldsymbol{r} + d$ is defined as

$$\begin{aligned}\Theta(s) &= E\{\exp(sQ)\} \\ &= E\{\exp[s(\boldsymbol{r}^T\boldsymbol{\Psi}\boldsymbol{r} + \boldsymbol{g}^T\boldsymbol{r} + d)]\}. \end{aligned} \tag{98}$$

According to Theorem (3.2a.1) in [18], if $\boldsymbol{\Psi}$ is a real symmetric matrix, then the MGF is

$$\begin{aligned}\Theta(s) &= |\boldsymbol{I} - 2s\boldsymbol{\Psi}\boldsymbol{C}|^{-\frac{1}{2}} \\ &\quad \exp\left\{-\frac{1}{2}(\boldsymbol{\mu}^T\boldsymbol{C}^{-1}\boldsymbol{\mu} - 2sd) + \frac{1}{2}(\boldsymbol{\mu} + s\boldsymbol{C}\boldsymbol{g})^T \right. \\ &\quad \left. \times(\boldsymbol{I} - 2s\boldsymbol{\Psi}\boldsymbol{C})^{-1}\boldsymbol{C}^{-1}(\boldsymbol{\mu} + s\boldsymbol{C}\boldsymbol{g})\right\} \qquad (99) \\ &= \left|\boldsymbol{I} - 2s\boldsymbol{C}^{\frac{1}{2}}\boldsymbol{\Psi}\boldsymbol{C}^{\frac{1}{2}}\right|^{-\frac{1}{2}} \\ &\quad \times \exp\left\{s(d + \boldsymbol{\mu}^T\boldsymbol{\Psi}\boldsymbol{\mu} + \boldsymbol{g}^T\boldsymbol{\mu}) \right. \\ &\quad + (s^2/2)\left(\boldsymbol{C}^{\frac{1}{2}}\boldsymbol{g} + 2\boldsymbol{C}^{\frac{1}{2}}\boldsymbol{\Psi}\boldsymbol{\mu}\right)^T \\ &\quad \left. \times\left(\boldsymbol{I} - 2s\boldsymbol{C}^{\frac{1}{2}}\boldsymbol{\Psi}\boldsymbol{C}^{\frac{1}{2}}\right)^{-1}\left(\boldsymbol{C}^{\frac{1}{2}}\boldsymbol{g} + 2\boldsymbol{C}^{\frac{1}{2}}\boldsymbol{\Psi}\boldsymbol{\mu}\right)\right\}. \qquad (100)\end{aligned}$$

Both equivalent forms (99) and (100) can be useful. Equation (99) does not require the square root $\boldsymbol{C}^{1/2}$, but the matrix $(\boldsymbol{I}-2s\boldsymbol{\Psi C})$ is asymmetric, whereas (100) does require $\boldsymbol{C}^{1/2}$, but the symmetry of $(\boldsymbol{I}-2s\boldsymbol{C}^{1/2}\boldsymbol{\Psi C}^{1/2})$ can lead to efficient calculation of the inverse and determinant.

We can also obtain a form without $\boldsymbol{C}^{1/2}$. Noting that $|\boldsymbol{I}-2s\boldsymbol{C}^{1/2}\boldsymbol{\Psi C}^{1/2}|=|\boldsymbol{I}-2s\boldsymbol{C\Psi}|$, and

$$\begin{aligned}\boldsymbol{C}^{\frac{1}{2}}\left(\boldsymbol{I}-2s\boldsymbol{C}^{\frac{1}{2}}\boldsymbol{\Psi C}^{\frac{1}{2}}\right)^{-1}\boldsymbol{C}^{\frac{1}{2}}&=(\boldsymbol{C}^{-\frac{1}{2}}-2s\boldsymbol{C}^{\frac{1}{2}}\boldsymbol{\Psi})^{-1}\boldsymbol{C}^{\frac{1}{2}}\\&=(\boldsymbol{I}-2s\boldsymbol{C\Psi})^{-1}\boldsymbol{C},\end{aligned}$$

then (100) can be expressed as

$$\begin{aligned}\Theta(s)=|\boldsymbol{I}-2s\boldsymbol{C\Psi}|^{-(1/2)}&\exp\{s(d+\boldsymbol{\mu}^T\boldsymbol{\Psi\mu}+\boldsymbol{g}^T\boldsymbol{\mu})\\&+(s^2/2)(\boldsymbol{g}+2\boldsymbol{\Psi\mu})^T(\boldsymbol{I}-2s\boldsymbol{C\Psi})^{-1}\boldsymbol{C}(\boldsymbol{g}+2\boldsymbol{\Psi\mu})\}.\end{aligned}\quad(101)$$

If $\boldsymbol{g}=\boldsymbol{0}$ and $d=0$, then Q degrades to $Q=\boldsymbol{r}^T\boldsymbol{\Psi r}$. In this case, $\Theta(s)$ of Q is given by

$$\begin{aligned}\Theta(s)=&\left|\boldsymbol{I}-2s\boldsymbol{C}^{\frac{1}{2}}\boldsymbol{\Psi C}^{\frac{1}{2}}\right|^{-\frac{1}{2}}\\&\times\exp\left\{s\boldsymbol{\mu}^T\boldsymbol{C}^{-\frac{1}{2}}\left(\boldsymbol{C}^{\frac{1}{2}}\boldsymbol{\Psi C}^{\frac{1}{2}}\right)\right.\\&\left.\times\left(\boldsymbol{I}-2s\boldsymbol{C}^{\frac{1}{2}}\boldsymbol{\Psi C}^{\frac{1}{2}}\right)^{-1}\boldsymbol{C}^{-\frac{1}{2}}\boldsymbol{\mu}\right)\right\}\end{aligned}\quad(102)$$

according to the last equality of $M_Q(t)$ in [18, p. 40].

When $\boldsymbol{\Psi}$ is asymmetric, since $\boldsymbol{r}^T\boldsymbol{\Psi r}=\boldsymbol{r}^T\boldsymbol{\Psi}^T\boldsymbol{r}$, we have an equivalent expression for Q as $Q=(1/2)\boldsymbol{r}^T(\boldsymbol{\Psi}+\boldsymbol{\Psi}^T)\boldsymbol{r}+\boldsymbol{g}^T\boldsymbol{r}+d$. Therefore, the above results are also applicable after replacing $\boldsymbol{\Psi}$ by $(1/2)(\boldsymbol{\Psi}+\boldsymbol{\Psi}^T)$.

B. Taylor Expansion of the Inverse and Determinant of a Matrix

Let square matrix $\boldsymbol{B}$ have a second order expansion for small α given by $\boldsymbol{B}=\boldsymbol{A}+\alpha\boldsymbol{X}+\alpha^2\boldsymbol{Y}$, where $\boldsymbol{A}$ is non-singular. Expansion of $\boldsymbol{B}^{-1}$ in a power series of α requires derivatives of $\boldsymbol{B}^{-1}$ with respect to α. Since $\boldsymbol{BB}^{-1}=\boldsymbol{I}$, we have

$$\boldsymbol{B}\frac{d\boldsymbol{B}^{-1}}{d\alpha}+\frac{d\boldsymbol{B}}{d\alpha}\boldsymbol{B}^{-1}=\boldsymbol{0}$$

which leads to

$$\frac{d\boldsymbol{B}^{-1}}{d\alpha}=-\boldsymbol{B}^{-1}\frac{d\boldsymbol{B}}{d\alpha}\boldsymbol{B}^{-1}.\quad(103)$$

$$\begin{aligned}\frac{d^2\boldsymbol{B}^{-1}}{d\alpha^2}&=-\frac{d\boldsymbol{B}^{-1}}{d\alpha}\frac{d\boldsymbol{B}}{d\alpha}\boldsymbol{B}^{-1}-\boldsymbol{B}^{-1}\frac{d^2\boldsymbol{B}}{d\alpha^2}\boldsymbol{B}^{-1}\\&\quad-\boldsymbol{B}^{-1}\frac{d\boldsymbol{B}}{d\alpha}\frac{d\boldsymbol{B}^{-1}}{d\alpha}\\&=2\boldsymbol{B}^{-1}\frac{d\boldsymbol{B}}{d\alpha}\boldsymbol{B}^{-1}\frac{d\boldsymbol{B}}{d\alpha}\boldsymbol{B}^{-1}-\boldsymbol{B}^{-1}\frac{d^2\boldsymbol{B}}{d\alpha^2}\boldsymbol{B}^{-1}\\&=2\boldsymbol{B}^{-1}\boldsymbol{X}\boldsymbol{B}^{-1}\boldsymbol{X}\boldsymbol{B}^{-1}-2\boldsymbol{B}^{-1}\boldsymbol{Y}\boldsymbol{B}^{-1}.\end{aligned}\quad(104)$$

Therefore, $\boldsymbol{B}^{-1}$ has a Taylor expansion given by

$$\begin{aligned}\boldsymbol{B}^{-1}=\boldsymbol{B}^{-1}|_{\alpha=0}+\alpha\frac{d\boldsymbol{B}^{-1}}{d\alpha}\bigg|_{\alpha=0}+\frac{1}{2}\alpha^2\frac{d^2\boldsymbol{B}^{-1}}{d\alpha^2}\bigg|_{\alpha=0}\\+\boldsymbol{O}(\alpha^3)\\=\boldsymbol{A}^{-1}-\alpha\boldsymbol{A}^{-1}\boldsymbol{X}\boldsymbol{A}^{-1}\\+\alpha^2[\boldsymbol{A}^{-1}(\boldsymbol{X}\boldsymbol{A}^{-1})^2-\boldsymbol{A}^{-1}\boldsymbol{Y}\boldsymbol{A}^{-1}]+\boldsymbol{O}(\alpha^3).\end{aligned}\quad(105)$$

The expansion of the determinant $|\boldsymbol{B}|$ requires associated derivatives as well. From (A.390) in [23, App. A]

$$\frac{d|\boldsymbol{B}|}{d\alpha}=|\boldsymbol{B}|\frac{d\ln|\boldsymbol{B}|}{d\alpha}=|\boldsymbol{B}|\mathrm{tr}\left(\boldsymbol{B}^{-1}\frac{d\boldsymbol{B}}{d\alpha}\right)$$

so that

$$\begin{aligned}\frac{d^2|\boldsymbol{B}|}{d\alpha^2}&=\frac{d|\boldsymbol{B}|}{d\alpha}\mathrm{tr}\left(\boldsymbol{B}^{-1}\frac{d\boldsymbol{B}}{d\alpha}\right)\\&\quad+|\boldsymbol{B}|\mathrm{tr}\left(\frac{d\boldsymbol{B}^{-1}}{d\alpha}\frac{d\boldsymbol{B}}{d\alpha}+\boldsymbol{B}^{-1}\frac{d^2\boldsymbol{B}}{d\alpha^2}\right)\\&=|\boldsymbol{B}|\mathrm{tr}^2\left(\boldsymbol{B}^{-1}\frac{d\boldsymbol{B}}{d\alpha}\right)\\&\quad+|\boldsymbol{B}|\mathrm{tr}\left(-\left(\boldsymbol{B}^{-1}\frac{d\boldsymbol{B}}{d\alpha}\right)^2+\boldsymbol{B}^{-1}\frac{d^2\boldsymbol{B}}{d\alpha^2}\right).\end{aligned}\quad(106)$$

Therefore, $|\boldsymbol{B}|$ has the following expansion:

$$\begin{aligned}|\boldsymbol{B}|&=|\boldsymbol{B}|_{\alpha=0}+\alpha\frac{d|\boldsymbol{B}|}{d\alpha}|_{\alpha=0}\\&\quad+\frac{1}{2}\alpha^2\frac{d^2|\boldsymbol{B}|}{d\alpha^2}|_{\alpha=0}+O(\alpha^3)\\&=|\boldsymbol{A}|+\alpha|\boldsymbol{A}|\mathrm{tr}(\boldsymbol{A}^{-1}\boldsymbol{X})\\&\quad+\frac{\alpha^2}{2}|\boldsymbol{A}|\{\mathrm{tr}^2[\boldsymbol{A}^{-1}\boldsymbol{X}]+\mathrm{tr}[2\boldsymbol{A}^{-1}\boldsymbol{Y}-(\boldsymbol{AX})^2]\}\\&\quad+O(\alpha^3).\end{aligned}\quad(107)$$

If $\boldsymbol{A}=\boldsymbol{I}$, then

$$\begin{aligned}&(\boldsymbol{I}+\alpha\boldsymbol{X}+\alpha^2\boldsymbol{Y})^{-1}\\&\quad=\boldsymbol{I}-\alpha\boldsymbol{X}+\alpha^2(\boldsymbol{X}^2-\boldsymbol{Y})+\boldsymbol{O}(\alpha^3).\end{aligned}\quad(108)$$

$$\begin{aligned}&|\boldsymbol{I}+\alpha\boldsymbol{X}+\alpha^2\boldsymbol{Y}|\\&\quad=1+\alpha\mathrm{tr}(\boldsymbol{X})+\frac{\alpha^2}{2}\{\mathrm{tr}^2(\boldsymbol{X})+\mathrm{tr}(2\boldsymbol{Y}-\boldsymbol{X}^2)\}+O(\alpha^3).\end{aligned}\quad(109)$$

The above also readily leads to

$$\begin{aligned}|\boldsymbol{I}+\alpha\boldsymbol{X}+\alpha^2\boldsymbol{Y}|^{-\frac{1}{2}}&=1-\frac{\alpha}{2}\mathrm{tr}(\boldsymbol{X})\\&\quad+\frac{\alpha^2}{4}\left[\frac{1}{2}\mathrm{tr}^2(\boldsymbol{X})-\mathrm{tr}(2\boldsymbol{Y}-\boldsymbol{X}^2)\right]+O(\alpha^3).\end{aligned}\quad(110)$$

APPENDIX II
EXAMPLE SIGNALS AND THEIR AUTOCORRELATION AND BANDWIDTH EXPRESSIONS

In our examples, we adopt mean-square bandwidth (MSB) defined by [24]

$$B^2=\int_{-\infty}^{\infty}\frac{|\dot{p}(t)|^2}{R(0)(2\pi)^2}dt=\int_{-\infty}^{\infty}\frac{f^2|P(f)|^2}{\beta(0)}df\quad(111)$$

where $p(t)$ and $P(f)$ are, respectively, the time and frequency-domain expressions of the signal, and $\beta(t)$ is the autocorrela-

tion. B is also known as the root-mean-square equivalent bandwidth (RMSB).

A. Square-Root Raised Cosine Pulse

The spectrum of a square-root raised cosine (SRRC) pulse is given by [4]

$$P_{\mathrm{SRRC}}(f) = \begin{cases} \sqrt{T_p/2}, & 0 \leqslant |f| \leqslant \frac{1-\tilde{\beta}}{T_p} \\ \sqrt{\frac{T_p}{4}\left\{1+\cos\left[\frac{\pi T_p}{2\tilde{\beta}}\left(|f|-\frac{1-\tilde{\beta}}{T_p}\right)\right]\right\}}, & \frac{1-\tilde{\beta}}{T_p} \leqslant |f| \leqslant \frac{1+\tilde{\beta}}{T_p} \\ 0, & |f| > \frac{1+\tilde{\beta}}{T_p}. \end{cases} \tag{112}$$

where $T_p/2$ is the first zero-crossing time, and $\tilde{\beta}$ is the roll-off factor. The time-domain expression is

$$p_{\mathrm{SRRC}}(t) = \begin{cases} \frac{\sin\left[\pi(1-\tilde{\beta})\frac{2t}{T_p}\right]+\frac{8\tilde{\beta}t}{T_p}\cos\left[2\pi(1+\tilde{\beta})\frac{t}{T_p}\right]}{\frac{2\pi t}{T_p}\left[1-\left(\frac{8\tilde{\beta}t}{T_p}\right)^2\right]}, & t \neq 0,\ t \neq \pm\frac{T_p}{8\tilde{\beta}}, \\ 1-\tilde{\beta}+\frac{4\tilde{\beta}}{\pi},\ t=0, \\ \frac{\tilde{\beta}}{\sqrt{2}}\left[\left(1+\frac{2}{\pi}\right)\sin\left(\frac{\pi}{4\tilde{\beta}}\right)+\left(1-\frac{2}{\pi}\right)\cos\left(\frac{\pi}{4\tilde{\beta}}\right)\right], & t=\pm\frac{T_p}{8\tilde{\beta}}. \end{cases} \tag{113}$$

The autocorrelation and squared MSB of the SRRC pulse are

$$\beta_{\mathrm{SRRC}}(\tau) = \mathrm{sinc}\left(\frac{2\tau}{T_p}\right)\frac{\cos(2\pi\tilde{\beta}\tau/T_p)}{1-(4\tilde{\beta}\tau/T_p)^2}$$
$$B^2_{\mathrm{SRRC}} = \frac{1}{3T_p^2}\left[1+\tilde{\beta}^2\left(3-\frac{24}{\pi^2}\right)\right]. \tag{114}$$

where $\mathrm{sinc}(x) \triangleq (\sin(\pi x))/(\pi x)$.

B. Gaussian Pulse

The Gaussian pulse, its spectrum and autocorrelation are [25]

$$p_{\mathrm{G}}(t) = \pm c\frac{1}{\sqrt{2\pi\sigma^2}}e^{-\frac{t^2}{2\sigma^2}} = \pm c\frac{\sqrt{2}}{\tilde{\alpha}}e^{-\frac{2\pi t^2}{\tilde{\alpha}^2}}$$
$$P_{\mathrm{G}}(f) = ce^{-\frac{\pi}{2}\tilde{\alpha}^2 f^2}, \beta_{\mathrm{G}}(\tau) = \frac{c^2}{\tilde{\alpha}}e^{-\frac{\pi}{\tilde{\alpha}^2}\tau^2} \tag{115}$$

where $\tilde{\alpha} \triangleq 4\pi\sigma^2$. We set $c^2 = \tilde{\alpha}$ for normalizing the autocorrelation, which makes $\beta_{\mathrm{G}}(0) = 1$ and does not affect the bandwidth. The squared MSB of the Gaussian pulse is obtained by the second-order moment of the Gaussian distribution as

$$B^2_{\mathrm{G}} = \int_{-\infty}^{\infty} f^2 \left|P_{\mathrm{G}}(f)\right|^2 df = \frac{1}{2\pi\tilde{\alpha}^2}. \tag{116}$$

C. Gaussian Doublet Pulse

The Gaussian doublet pulse (the second derivative of the Gaussian pulse) is a common pulse in UWB systems, given by [25]

$$p_{\mathrm{G2}}(t) = \frac{d^2 p_{\mathrm{G}}(t)}{dt^2} = cK\left(1-\frac{4\pi}{\tilde{\alpha}^2}t^2\right)e^{-\frac{2\pi}{\tilde{\alpha}^2}t^2} \tag{117}$$

where $K = -\sqrt{32}\pi/\tilde{\alpha}^3 = -1/\sqrt{2\pi}\sigma^3$ is a coefficient inherited from the above Gaussian pulse. Its autocorrelation is

$$\beta_{\mathrm{G2}}(\tau) = \frac{d^4\beta_{\mathrm{G}}(\tau)}{d\tau^4} = c^2K^2\left(\frac{\pi^2}{2\tilde{\alpha}^3}\tau^4 - \frac{3\pi}{2\tilde{\alpha}}\tau^2 + \frac{3\tilde{\alpha}}{8}\right)e^{-\frac{\pi}{\tilde{\alpha}^2}\tau^2}. \tag{118}$$

To normalize we set $c^2K^2 = 8/(3\tilde{\alpha})$. The spectrum of the pulse and its squared MSB are given by [25]

$$P_{\mathrm{G2}}(f) = c(j2\pi f)^2 e^{-\frac{\pi}{2}\tilde{\alpha}^2 f^2}$$
$$B^2_{\mathrm{G2}} = \int_{-\infty}^{\infty} f^2 |P_{\mathrm{G2}}(f)|^2 df = \frac{5}{2\pi\tilde{\alpha}^2}. \tag{119}$$

D. Square-Root Raised Cosine Pulse Modulated by a PN Code

The SRRC pulse modulated by a pseudorandom noise (PN) code generates a pulse train. Suppose the code has N chips with a duration of T_c for each chip. The SRRC pulse with the first zero-crossing point $T_p/2$ is cut at $\pm(T_c)/(2) \geqslant 3T_p$. We choose pseudo-random m-sequences of length 15, corresponding to the generating polynomial $g(x) = x^4+x^3+1$. The discrete periodic autocorrelation of binary (± 1) m-sequence is [26]

$$\theta(k) = \frac{1}{N}\sum_{n=0}^{N-1} c_n c_{n+k} = \begin{cases} 1, & k = \tilde{L}N \\ -\frac{1}{N}, & k \neq \tilde{L}N \end{cases} \tag{120}$$

where $\tilde{L}$ is an integer. The pulse train and autocorrelation are given by

$$p_{\mathrm{PN}}(t) = \sum_{i=0}^{N-1} c_i p_{\mathrm{SRRC}}(t-iT_c) \tag{121}$$

$$\beta_{\mathrm{PN}}(\tau) = \int_{-\infty}^{\infty} p_{\mathrm{PN}}(t)p_{\mathrm{PN}}(t+\tau)dt = \sum_{i=0}^{N-1}\sum_{j=0}^{N-1} c_i c_j \int_{-\infty}^{\infty} p_{\mathrm{SRRC}} \times (t-iT_c)p_{\mathrm{SRRC}}(t-jT_c+\tau)dt. \tag{122}$$

The delay τ can be expressed as $\tau = kT_c + \tau_\epsilon$, where $0 \leq \tau_\epsilon < T_c$, and then the SRRC pulses overlap only for $j = k+m$ and $j = k+m+1$. So the autocorrelation of the PN pulse train becomes [26]

$$\beta_{\mathrm{PN}}(\tau) = \beta_{\mathrm{PN}}(k,\tau_\epsilon) = \theta(k)\cdot\beta_{\mathrm{SRRC}}(\tau_\epsilon) + \theta(k+1)\beta_{\mathrm{SRRC}}(T_c-\tau_\epsilon). \tag{123}$$

ACKNOWLEDGMENT

The authors would like to thank R. Kozick for his significant contributions to this work.

REFERENCES

[1] B. M. Sadler, N. Liu, and Z. Xu, "Ziv–Zakai bound on time delay estimation in unknown convolutive random channels," presented at the IEEE Sensor Array Multichannel Signal Processing Workshop, Darmstadt, Germany, Jul. 21–23, 2008.

[2] S. F. Yau and Y. Bresler, "A compact Cramér–Rao bound expression for parametric estimation of superimposed signals," *IEEE Trans. Signal Process.*, vol. 40, no. 5, pp. 1226–1230, May 1992.

[3] H. Saarnisaari, "ML time delay estimation in a multipath channel," in *Proc. IEEE 4th Int. Symp. Spread Spectrum Tech. Appl.*, Sep. 1996, pp. 1007–1011.
[4] J. G. Proakis, *Digital Communications*, 4th ed. New York: McGraw-Hill, 2000, pp. 546–547.
[5] M. K. Simon and M.-S. Alouini, *Digital Communication over Fading Channels: A Unified Approach to Performance Analysis*, 2nd ed. New York: Wiley, 2005.
[6] U. G. Schuster and H. Bolcskei, "Ultra-wideband channel modeling on the basis of information-theoretic criteria," *IEEE Trans. Wireless Commun.*, vol. 6, no. 7, pp. 2464–2475, Jul. 2007.
[7] D. Chazan, M. Zakai, and J. Ziv, "Improved lower bounds on signal parameter estimation," *IEEE Trans. Inf. Theory*, vol. 21, no. 1, pp. 90–93, Jan. 1975.
[8] J. Ziv and M. Zakai, "Some lower bounds on signal parameter estimation," *IEEE Trans. Inf. Theory*, vol. IT-15, no. 3, pp. 386–391, May 1969.
[9] H. L. Van Trees and K. L. Bell, *Bayesian Bounds for Parameter Estimation and Nonlinear Filtering/Tracking*. New York: Wiley, 2007, pp. 1–62.
[10] B. M. Sadler and R. J. Kozick, "A survey of time delay estimation performance bounds," in *Proc. 4th IEEE Workshop Sensor Array Multichannel Signal Processing (SAM)*, Jul. 2006, pp. 282–288, Invited.
[11] R. J. Kozick and B. M. Sadler, "Frequency hopping waveform diversity for time delay estimation," in *Proc. Int. Waveform Diversity and Design Conf.*, Jan. 2006.
[12] R. J. Kozick and B. M. Sadler, "Bounds and algorithms for time delay estimation on parallel, flat fading channels," in *Proc. IEEE Intl. Conf. Acoustics, Speech, Signal Processing*, Apr. 2008, pp. 2413–2416.
[13] R. J. Kozick and B. M. Sadler, "Communications channel estimation and waveform design: Time delay estimation on parallel, flat fading channels," Army Research Lab., Adelphi, MD, Tech. Rep. ARL-TR-5046, Feb. 2010.
[14] B. M. Sadler, L. Huang, and Z. Xu, "Ziv–Zakai time delay estimation bound for ultra-wideband signals," presented at the IEEE Int. Conf. Acoustics, Speech, Signal Processing, Honolulu, HI, Apr. 15–20, 2007.
[15] E. Weinstein and A. J. Weiss, "A general class of lower bounds in parameter estimation," *IEEE Trans. Inf. Theory*, vol. 34, pp. 338–342, Mar. 1988.
[16] Z. Xu and B. M. Sadler, "Time delay estimation bounds in convolutive random channels," *IEEE J. Sel. Topics Signal Process. (Special Issue on Performance Limits of Ultra-Wideband Systems)*, vol. 1, no. 3, pp. 418–430, Oct. 2007.
[17] H. L. Van Trees, *Detection, Estimation, and Modulation Theory: Part I—Detection, Estimation, and Linear Modulation Theory*. New York: Wiley, 2001, ch. 4.
[18] A. M. Mathai and S. B. Provost, *Quadratic Forms in Random Variables: Theory and Applications*. New York: Marcel Dekker, 1992.
[19] Z. Xu, "Perturbation analysis for subspace decomposition with applications in subspace-based algorithms," *IEEE Trans. Signal Process.*, vol. 50, no. 11, pp. 2820–2830, Nov. 2002.
[20] S. M. Kay, *Fundamentals of Statistical Processing, Volume I: Estimation Theory*. Englewood Cliffs, NJ: Prentice-Hall, 1993.
[21] M. Z. Win and R. A. Scholtz, "Characterization of ultra-wide bandwidth wireless indoor channels: A communication-theoretic view," *IEEE J. Sel. Areas Commun.*, vol. 20, pp. 1613–1627, Dec. 2002.
[22] E. Weinstein and A. Weiss, "Fundamental limitations in passive time delay estimation—Part II: Wideband systems," *IEEE Trans. Acoust. Speech, Signal Process.*, vol. 32, pp. 1064–1078, Oct. 1984.
[23] H. L. Van Trees, *Detection, Estimation, and Modulation Theory: Part IV—Optimum Array Processing*. New York: Wiley, 2002.
[24] A. H. Nuttall, "Minimum rms bandwidth of M time-limited signals with specified code or correlation matrix," *IEEE Trans. Inf. Theory*, vol. IT-14, pp. 699–707, Sep. 1968.
[25] M. Ghavami, L. Michael, and R. Kohno, *Ultra Wideband Signals and Systems in Communication Engineering*, 2nd ed. New York: Wiley, 2007, pp. 28–31.
[26] R. L. Peterson, R. E. Ziemer, and D. E. Borth, *Introduction to Spread Spectrum Communications*. Englewood Cliffs, NJ: Prentice-Hall, 1995, pp. 90–91.

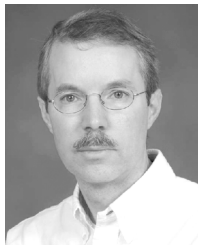

Brian M. Sadler (S'81–M'81–SM'02–F'07) received the B.S. and M.S. degrees from the University of Maryland, College Park, and the Ph.D. degree from the University of Virginia, Charlottesville, all in electrical engineering.

He is a Senior Research Scientist at the Army Research Laboratory (ARL), Adelphi, MD. His research interests include information science, networked and autonomous systems, acoustics, optics, and mixed-signal integrated circuit architectures. He has coauthored more than 270 publications and several patents in these areas.

Dr. Sadler is an Associate Editor for *EURASIP Signal Processing* and was an Associate Editor for the IEEE TRANSACTIONS ON SIGNAL PROCESSING and the IEEE SIGNAL PROCESSING LETTERS, and has been a Guest Editor for several journals, including the IEEE JOURNAL ON SELECTED TOPICS IN SIGNAL PROCESSING, the IEEE JOURNAL ON SELECTED AREAS IN COMMUNICATIONS, and the *IEEE Signal Processing Magazine*. He is a member of the IEEE Signal Processing Society Sensor Array and Multi-Channel Technical Committee and has been active in IEEE conference planning and organization for many years. He received a Best Paper Award (with R. Kozick) from the Signal Processing Society in 2006. He has received several ARL and Army R&D awards, as well as a 2008 Outstanding Invention of the Year Award from the University of Maryland (with J. Baras and P. Yu).

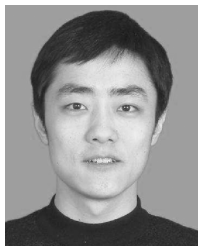

Ning Liu (S'08) received the B.S. and M.S. degrees in communication engineering from Xidian University, Xi'an, China, in 2000 and 2003, respectively. He is currently working towards the Ph.D. degree in electrical engineering at the University of California, Riverside.

From 2003 to 2006, he was a System Engineer at Datang Mobile Communications Equipment Company, Beijing, China. His research interests include statistical signal processing, transceiver design for wireless communication systems, cooperative localization and tracking for cellular and wireless sensor networks, and time delay estimation.

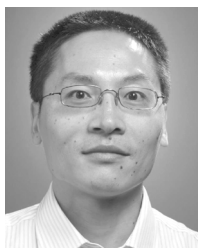

Zhengyuan Xu (S'97–M'99–SM'02) received the B.E. and M.E. degrees in electronic engineering from Tsinghua University, Beijing, China, in 1989 and 1991, respectively, and the Ph.D. degree in electrical engineering from Stevens Institute of Technology, Hoboken, NJ, in 1999.

From 1991 to 1996, he was a System Engineer and Department Manager at the Tsinghua Unisplendour Group Corporation, Tsinghua University. Since 1999, he has been a faculty member in the Department of Electrical Engineering, University of California, Riverside, where he is currently a Professor with tenure. He is Director of the Multi-Campus Center for Ubiquitous Communication by Light (UC-Light) funded by the University of California Office of the President. He has held visiting positions at Stanford University and the University of Science and Technology of China. His research interests lie in wireless communications, networking, and signal processing. They include multiuser spread spectrum, impulse radio, ultra-wideband, wireless ultraviolet and visible light communication, geolocation, navigation, optical imaging and sensing, hybrid radio and optical communication, sensor and ad hoc networks.

Dr. Xu has served as an associate editor and guest editor for various IEEE journals in communications, vehicle technology, or signal processing. He has served as a chair, session chair, technical program chair, and technical program committee member for many international conferences. He was also an elected member of the IEEE Signal Processing Society's Technical Committee on Signal Processing for Communications in the past six years. He received the Outstanding Student Award and the Motorola Scholarship from Tsinghua University, and the Peskin Award from the Stevens Institute of Technology. He also received the Academic Senate Research Award and the Regents' Faculty Award from the University of California, Riverside.